Cell Reports

Article

Excessive Astrocytic GABA Causes Cortical Hypometabolism and Impedes Functional Recovery after Subcortical Stroke

Graphical Abstract

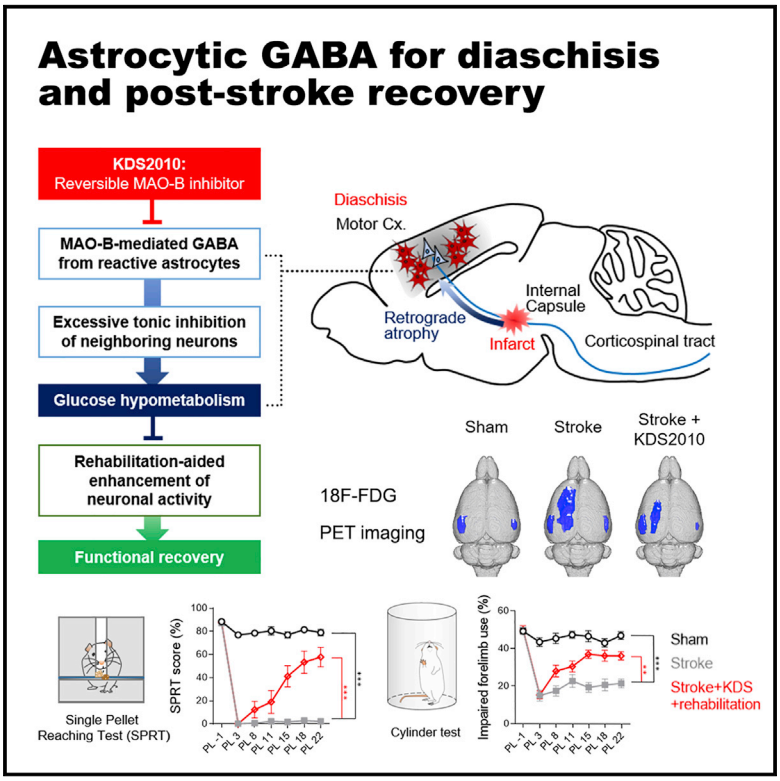

Highlights

- Capsular infarct induces neuronal atrophy and reactive astrogliosis in motor cortex
- Tonic GABA from reactive astrocytes suppresses neuronal glucose metabolism
- Inhibition of MAO-B, the GABA-synthesizing enzyme, restores glucose metabolism
- Combined therapy of MAO-B inhibitor and rehabilitation causes functional recovery

Authors

Min-Ho Nam, Jongwook Cho, Dae-Hyuk Kwon, ..., Mijin Yun, C. Justin Lee, Hyoung-Ihl Kim

Correspondence

cjl@ibs.re.kr (C.J.L.), hyoungihl@gist.ac.kr (H.-I.K.)

In Brief

Nam et al. demonstrate that excessive GABA from reactive astrocytes accounts for cortical glucose hypometabolism followed by subcortical stroke and impedes rehabilitation-aided motor functional recovery by aberrantly suppressing motor cortical neuronal activity. Thus, MAO-B, the astrocytic GABA-synthesizing enzyme, can be a therapeutic target for functional recovery after subcortical stroke.

Nam et al., 2020, Cell Reports *32*, 107861
July 7, 2020
https://doi.org/10.1016/j.celrep.2020.107861

CellPress

Cell Reports

CellPress
OPEN ACCESS

Article

Excessive Astrocytic GABA Causes Cortical Hypometabolism and Impedes Functional Recovery after Subcortical Stroke

Min-Ho Nam,[1,13] Jongwook Cho,[2,13] Dae-Hyuk Kwon,[2] Ji-Young Park,[2] Junsung Woo,[1] Jungmoo Lee,[1,3,4] Sangwon Lee,[5] Hae Young Ko,[5] Woojin Won,[1,3,4] Ra Gyung Kim,[2] Hanlim Song,[2] Soo-Jin Oh,[1,6] Ji Won Choi,[6] Ki Duk Park,[6,7] Eun Kyung Park,[8] Haejin Jung,[9] Hyung-Seok Kim,[10] Min-Cheol Lee,[11] Mijin Yun,[5] C. Justin Lee,[1,4,14,*] and Hyoung-Ihl Kim[2,12,*]

[1]Center for Neuroscience, Korea Institute of Science and Technology (KIST), Seoul 02792, Republic of Korea
[2]Department of Biomedical Science and Engineering, Gwangju Institute of Science and Technology (GIST), Gwangju 61005, Republic of Korea
[3]KU-KIST Graduate School of Converging Science of Technology, Korea University, Seoul 02841, Republic of Korea
[4]Center for Cognition and Sociality, Institute for Basic Science, Daejeon 34126, Republic of Korea
[5]Department of Nuclear Medicine, Severance Hospital, Yonsei University College of Medicine, Seoul 03722, Republic of Korea
[6]Convergence Research Center for Dementia, KIST, Seoul 02792, Republic of Korea
[7]KHU-KIST Department of Converging Science and Technology, Kyung Hee University, Seoul 02447, Republic of Korea
[8]Neurobiogen, Seongnam, Gyeonggi-do 13201, Republic of Korea
[9]Flow Cytometry Core Facility of Research Solution Center, Institute of Basic Science, Daejeon 34126, Republic of Korea
[10]Department of Legal Medicine, Chonnam National University Medical School, Gwangju 61469, Republic of Korea
[11]Department of Pathology, Chonnam National University Medical School, Gwangju 61469, Republic of Korea
[12]Departement of Neurosurgery, Presbyterian Medical Center, Jeonju 54987, Republic of Korea
[13]These authors contributed equally
[14]Lead Contact
*Correspondence: cjl@ibs.re.kr (C.J.L.), hyoungihl@gist.ac.kr (H.-I.K.)
https://doi.org/10.1016/j.celrep.2020.107861

SUMMARY

Glucose hypometabolism in cortical structures after functional disconnection is frequently reported in patients with white matter diseases such as subcortical stroke. However, the molecular and cellular mechanisms have been poorly elucidated. Here we show, in an animal model of internal capsular infarct, that GABA-synthesizing reactive astrocytes in distant cortical areas cause glucose hypometabolism via tonic inhibition of neighboring neurons. We find that reversal of aberrant astrocytic GABA synthesis, by pharmacological inhibition and astrocyte-specific gene silencing of MAO-B, reverses the reduction in cortical glucose metabolism. Moreover, induction of aberrant astrocytic GABA synthesis by cortical injection of putrescine or adenovirus recapitulates cortical hypometabolism. Furthermore, MAO-B inhibition causes a remarkable recovery from post-stroke motor deficits when combined with a rehabilitation regimen. Collectively, our data indicate that cortical glucose hypometabolism in subcortical stroke is caused by aberrant astrocytic GABA and MAO-B inhibition and that attenuating cortical hypometabolism can be a therapeutic approach in subcortical stroke.

INTRODUCTION

Subcortical stroke accounts for up to 30% of all ischemic strokes in humans (Sacco et al., 2006) and is known for its poor prognosis (Yamashita et al., 2016). In several white matter diseases, including subcortical stroke and vascular dementia, the presence of regional glucose hypometabolism in the cortex has been frequently reported (Chu et al., 2002; Tatsch et al., 2003). This regional glucose hypometabolism is an important characteristic of diaschisis, which is defined as a change in a distant area following a focal brain injury (Finger et al., 2004). The appearance of diaschisis has been closely associated with both clinical symptoms (Carrera and Tononi, 2014) and recovery from stroke (Seitz et al., 1999; Takasawa et al., 2002). However, because of the lack of proper animal models, little is known about the cellular and molecular etiology of cortical hypometabolism in subcortical stroke. Moreover, whether and how attenuating cortical hypometabolism can promote the functional recovery after subcortical stroke have been largely unexplored.

We have recently developed a rat model of capsular infarct using the focal photo-thrombosis technique and successfully reproduced an appearance of diaschisis in cortical areas (Kim et al., 2014, 2015). We reported that electrical stimulation of the cortical diaschisis region caused a significant reversal of

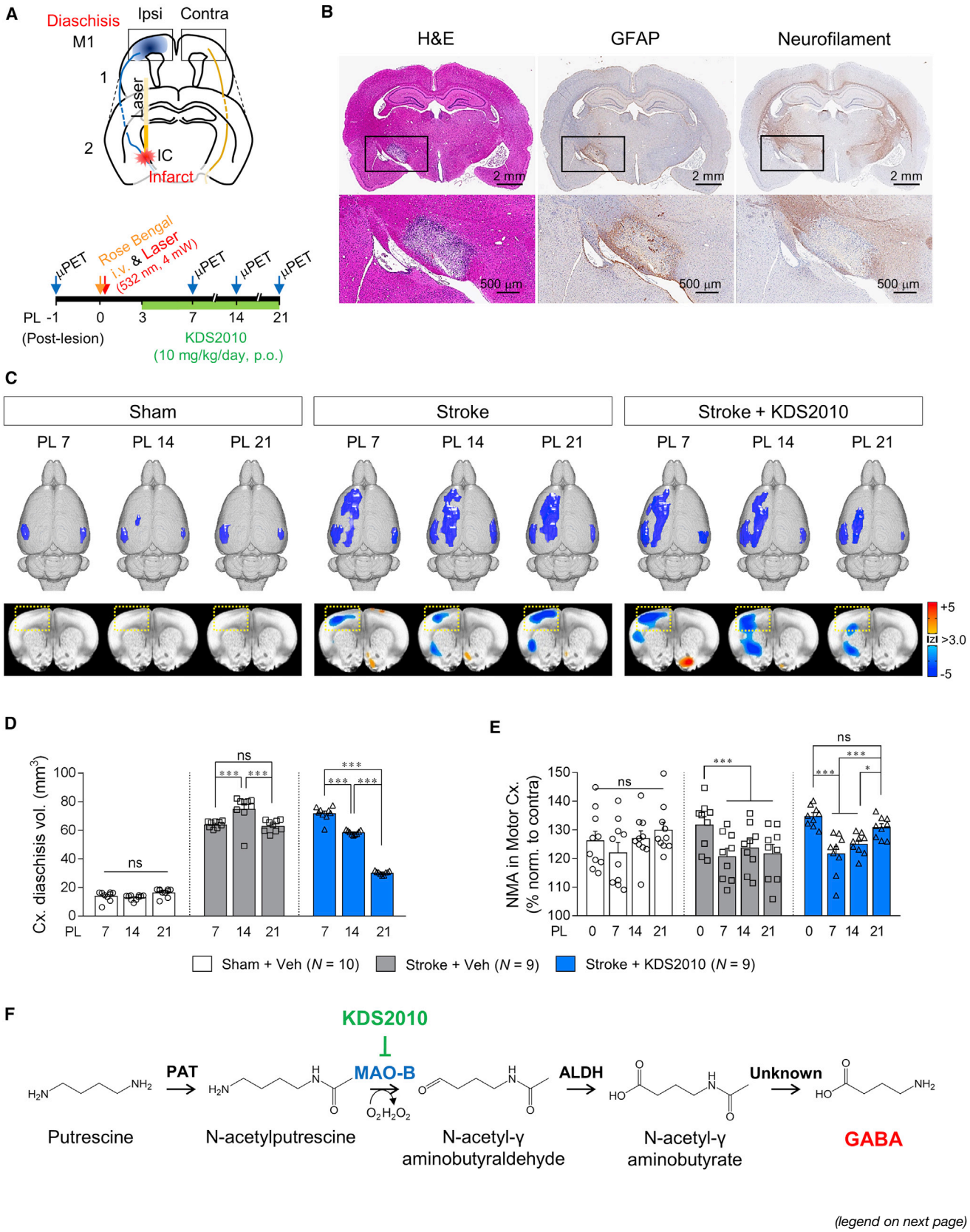

(legend on next page)

diaschisis and recovery from post-stroke motor deficits when combined with rehabilitation, while rehabilitation alone did not (Kim et al., 2016). However, how electrical stimulation caused the reversal of diaschisis was not revealed in the previous study. Given that cortical hypometabolism in diaschisis is tightly associated with reduced neuronal and synaptic activities (Lundgaard et al., 2015), here we postulate that the cortical hypometabolism is caused by the inhibitory action of GABA.

Astrogliosis, a characteristic reaction of astrocytes to an injury or disease with morphological alteration, has been reported to be present in the diaschisis region, as well as in the infarct areas of brains with stroke (Badan et al., 2003; Burda and Sofroniew, 2014; Garbuzova-Davis et al., 2013). In addition, we have previously reported that excessive GABA from reactive astrocytes aberrantly suppresses neighboring neuronal activity (Heo et al., 2020; Jo et al., 2014; Pandit et al., 2020; Shim et al., 2019; Yoon et al., 2014). Aberrant GABA synthesis in reactive astrocytes has been observed in the hippocampus in Alzheimer's disease mouse models and the temporal cortex in postmortem brains from Alzheimer's disease patients (Jo et al., 2014; Wu et al., 2014), the hippocampus in a kainate-induced seizure model (Pandit et al., 2020), the hypothalamus in an inflammatory cytokine-induced anxiety-like behavior model (Shim et al., 2019), and the substantia nigra pars compacta in various animal models and patients with Parkinson's disease (Heo et al., 2020). From these previous studies, we hypothesized that aberrant GABA synthesized and released from reactive astrocytes causes a reduction in regional metabolism in the diaschisis region by excessive GABA to inhibit the synaptic activity of neighboring cortical neurons. Furthermore, we tested the possibility that astrocytic GABA-mediated glucose hypometabolism impedes functional recovery by rehabilitation-mediated activation of motor circuits.

RESULTS

MAO-B as the Key Mediator for Glucose Hypometabolism

To monitor the generation and maintenance of diaschisis in the capsular infarct model with distinct damage of corticospinal motor fibers and astrogliosis in the internal capsule (Figures 1A and 1B), we performed longitudinal 2-deoxy-2-[^{18}F]-fluoro-D-glucose micro-positron emission tomography (FDG-microPET). We found that the ipsilesional cortices in the capsular infarct model displayed extensive glucose hypometabolism (i.e., diaschisis) at day 7 after stroke operation. This cortical glucose hypometabolism was sustained for more than 2 weeks, as evidenced by significantly increased cortical diaschisis volume, which did not appear in sham-operated animals (Figures 1C, 1D, and S1). We also found that infarction of the internal capsule significantly decreased normalized metabolic activity (NMA), which is each voxel's standardized uptake value (SUV) of FDG normalized to the averaged SUV throughout the whole brain, in the primary motor cortex (M1; Figures 1E and S1). M1 is a highly relevant brain region to post-stroke motor deficits (Li et al., 2016). Next, we tested whether excessive GABA synthesis from reactive astrocytes is the key mediator of diaschisis by using a recently developed selective and reversible inhibitor of monoamine oxidase-B (MAO-B), KDS2010, which has been confirmed to effectively block astrocytic GABA synthesis (Park et al., 2019). Intriguingly, we found a dramatic decrease of cortical diaschisis volume (Figure 1D) and a significant recovery of glucose metabolism in M1 by KDS2010 administration (Figures 1E and S1). These results suggest astrocytic GABA as the key mediator for cortical glucose hypometabolism.

Excessive GABA from Reactive Astrocytes in the Diaschisis Region

MAO-B is known as the key enzyme for astrocytic GABA synthesis through the putrescine degradation pathway (Yoon et al., 2014). Given that glucose hypometabolism is tightly associated with reduced synaptic activity (Lundgaard et al., 2015), the reversal of diaschisis by MAO-B inhibitor treatment is attributed to prevention of aberrant inhibition of synaptic activities by excessive GABA. Therefore, we examined astrocytic GABA in the diaschisis region by performing immunohistochemistry with antibodies against GABA and MAO-B. We found that immunoreactivities of GABA and MAO-B were significantly increased in reactive astrocytes in the diaschisis region in the capsular infarct model compared with sham-operated animals (Figures 2A, 2B, 2E, and S2). Astrocytic reactivity was defined by an increased ramification index assessed using Sholl analysis (Figures 2C and 2D), increased GFAP-positive area (Figure S2C), and increased mRNA levels of various markers for reactive astrocytes, such as GFAP, MAO-B, inducible nitric oxide synthase (iNOS) (Endoh et al., 1994), LCN2 (Bi et al., 2013), and vimentin (Mucke and Eddleston, 1993) (Figure S2G). On the other hand, we found no significant alteration of neuronal GABA (Figures S3A and S3B). Meanwhile, MAO-B inhibition by KDS2010 treatment significantly restored from aberrant astrocytic GABA (Figures 2C–2E), elevated protein level and enzymatic activity of MAO-B, and elevated mRNA levels of astrocytic reactivity markers (Figure S2). Notably, we found a significant negative correlation between astrocytic GABA level and NMA in the diaschisis region (Figure 2F), suggesting that astrocytic GABA suppresses glucose uptake. In the contralesional motor cortex,

Figure 1. A Reversible MAO-B Inhibitor Reverses Diaschisis in the Motor Cortex in a Capsular Infarct Model

(A) Schematic diagram of the capsular infarct model and timeline of experiments.

(B) Representative H&E-, GFAP-, and neurofilament-stained sections of internal capsule.

(C) FDG-microPET images of sham, stroke, and stroke with KDS2010 treatment.

(D) Cortical diaschisis volume ($F_{4, 50} = 121.1$, $p < 0.001$).

(E) Time-dependent change of NMA in motor cortex ($F_{6, 75} = 6.423$, $p < 0.001$).

(F) Biosynthetic mechanism of GABA through MAO-B in astrocytes.

N refers to the number of animals studied. For all panels, mean ± SEM, assessed using repeated-measures (RM) two-way ANOVA with Bonferroni test (*$p < 0.05$ and ***$p < 0.001$; ns, non-significant).

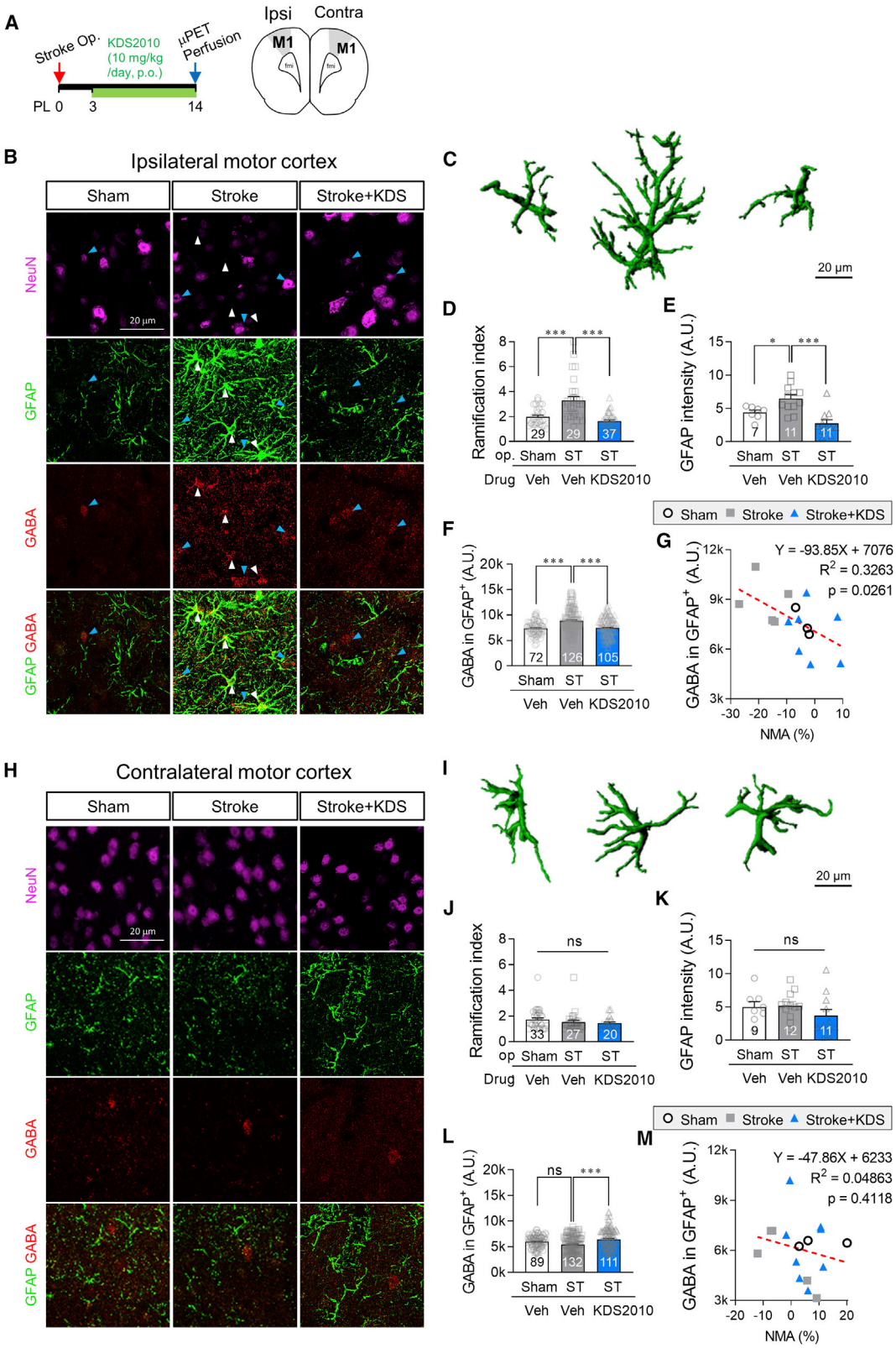

(legend on next page)

however, we could not observe alteration of astrocytic GABA or a correlation between astrocytic GABA and glucose uptake (Figures 2G–2K). In addition, KDS2010 treatment did not cause any alteration of morphology and GABA level of astrocytes in sham-operated animals (Figures S3C–S3H). These results indicate that cortical hypometabolism in the ipsilesional motor cortex following capsular infarct requires elevated astrocytic GABA produced in a MAO-B-dependent manner.

To directly test if reactive astrocytes excessively contain and release GABA at the single-cell level, we used the sniffer-patch technique with a biosensor for GABA to detect the release of GABA from an acutely dissociated astrocyte from the diaschisis region (Figure 3A), as previously described (Jo et al., 2014). Among the acutely dissociated cells from rat cortical tissues, a distinct population of GFAP-positive astrocytes (10.4%) was detected, while almost no neurons (0.04%) were detected (Figure S4A). The small proportion of GFAP-positive astrocytes among the whole acutely dissociated cells could be due to the low expression of GFAP in cortical astrocytes, as revealed by recent transcriptomic studies (Batiuk et al., 2020; Bayraktar et al., 2020), and this possibility should be tested in future investigations. The acutely dissociated cells were stimulated by pressure application of TFLLR, which is a peptide agonist of protease-activated receptor 1 (PAR1). Because only astrocytes, but not neurons, express PAR1 in the cortex, TFLLR has been reported to cause Ca^{2+} increase and transmitter release from astrocytes, but not neurons (Lee et al., 2007). We confirmed that a certain subpopulation of acutely dissociated cells responded to TFLLR by Ca^{2+} flux analysis using flow cytometry (Figure S4B), indicating the presence of functional astrocytes. We found that TFLLR caused a marked release of GABA from cortical astrocytes of the stroke rats, while GABA release was rarely observed in astrocytes in sham-operated rats (Figures 3B–3D). Nevertheless, it is still unclear that the GABA response is mediated by astrocytes, and it could be mediated by the 90% of GFAP-negative cells. Overall, these findings support our findings that reactive astrocytes in the diaschisis region contain and release an excessive amount of GABA, which can be readily released upon Ca^{2+} increase.

Excessive Tonic Inhibition by Aberrant Astrocytic GABA

We next asked whether excessive astrocytic GABA escalates the tonic inhibition of cortical pyramidal neurons in the diaschisis region. We performed whole-cell patch-clamp recordings from the pyramidal neurons in layer 2/3 of the ipsilesional motor cortex, where diaschisis was pre-identified by FDG-microPET. We measured $GABA_A$ receptor-mediated currents in the presence of the ionotropic glutamate receptor antagonists APV (50 μM) and CNQX (20 μM), as described previously (Lee et al., 2010) (Figure 3E). We found that the tonic GABA current, revealed by treatment with the $GABA_A$ receptor antagonist bicuculline (50 μM), was dramatically increased in the ipsilesional motor cortex of stroke-operated animals, which was successfully restored to the normal level by KDS2010 treatment (Figures 3F and 3G). On the other hand, we could not find any significant change in the frequency and amplitude of spontaneous inhibitory postsynaptic currents (sIPSCs) in all conditions (Figures 3H and 3L), suggesting that inhibitory action by neuronal phasic GABA was not altered. In the contralesional motor cortex, both tonic and phasic GABA currents were not altered (Figures 3J–3N). In addition, we found that excessive tonic GABA in the diaschisis region was attributed neither to increased expression of $GABA_AR\alpha5$ nor dysfunction of GAT-mediated GABA uptake (Figures S4C–S4J). Taken together, aberrant GABA from reactive astrocytes tonically inhibits the excitability of neighboring neurons in the ipsilesional motor cortex of the capsular infarct model, ultimately leading to cortical glucose hypometabolism.

Astrocytic GABA Is Necessary and Sufficient for Hypometabolism

We have demonstrated that MAO-B inhibition by systemic administration of KDS2010 reduced the extent and volume of diaschisis (Figure 1). To directly identify the cell type and region specificity of MAO-B's contribution to diaschisis, we performed astrocyte-specific gene silencing of MAO-B by injecting a mixture of AAV-GFAP-Cre-mCherry and lentivirus carrying pSico-MAO-B-shRNA-GFP (or pSico-scrambled-shRNA-GFP for control) into the motor cortex, where diaschisis is expected to be generated by a stroke operation (Figures 4A, S5A, and S5B). FDG-microPET revealed that subcortical stroke-induced cortical hypometabolism in the motor cortex was significantly decreased by astrocyte-specific gene silencing of MAO-B in the motor cortex, while scrambled short hairpin RNA (shRNA) injection did not rescue from hypometabolism (Figures 4B–4D). These findings indicate that astrocytic MAO-B in the motor cortex is necessary for the development of cortical hypometabolism. This astrocytic MAO-B-dependent reversal of diaschisis was associated with reduced astrocytic reactivity and GABA production (Figures S5C–S5F) and restored tonic GABA current, but not phasic GABA in the same gene-silenced region (Figures 4E–4H). In addition, astrocyte-specific gene silencing of Bestrophin 1 (Best1) (Figures S5G and S5H), a Ca^{2+}-activated anion channel that is the major GABA-releasing pathway in astrocytes (Jo et al., 2014; Lee et al., 2010; Oh and Lee, 2017), significantly

Figure 2. MAO-B-Dependent Excessive Astrocytic GABA Was Observed in Diaschisis

(A) Timeline of experiments and primary motor cortex (M1) as the region of interest (ROI).

(B and H) Representative confocal images of GFAP, GABA, and NeuN (n = 3, 5, and 7 for sham, stroke, and stroke + KDS groups, respectively).

(C and I) Representative three-dimensional (3D)-rendered astrocytes using Imaris 9.0.

(D and J) Ramification index of astrocytes (D, $F_{2, 92} = 20.89$, $p < 0.001$; J, $F_{2, 77} = 1,124$, $p = 0.330$).

(E and K) GFAP intensity (E, $F_{2, 27} = 13.12$, $p < 0.001$; K, $F_{2, 28} = 1.103$, $p = 0.346$).

(F and L) GABA intensity in GFAP-positive astrocytes (F, $F_{2, 300} = 19.54$, $p < 0.001$; L, $H = 14.93$, $p = 0.0006$).

(G and M) Linear regression of astrocytic GABA and NMA (G, $F_{1, 13} = 6.295$; M, $F_{1, 14} = 0.7156$).

Every point represents one animal. The number on each bar refers to the number of cells analyzed. N refers to the number of animals studied. For all panels, mean ± SEM, assessed using one-way ANOVA with Tukey test (D–F and J–L) or linear regression (G and M) (*$p < 0.05$, **$p < 0.01$, and ***$p < 0.001$; ns, non-significant).

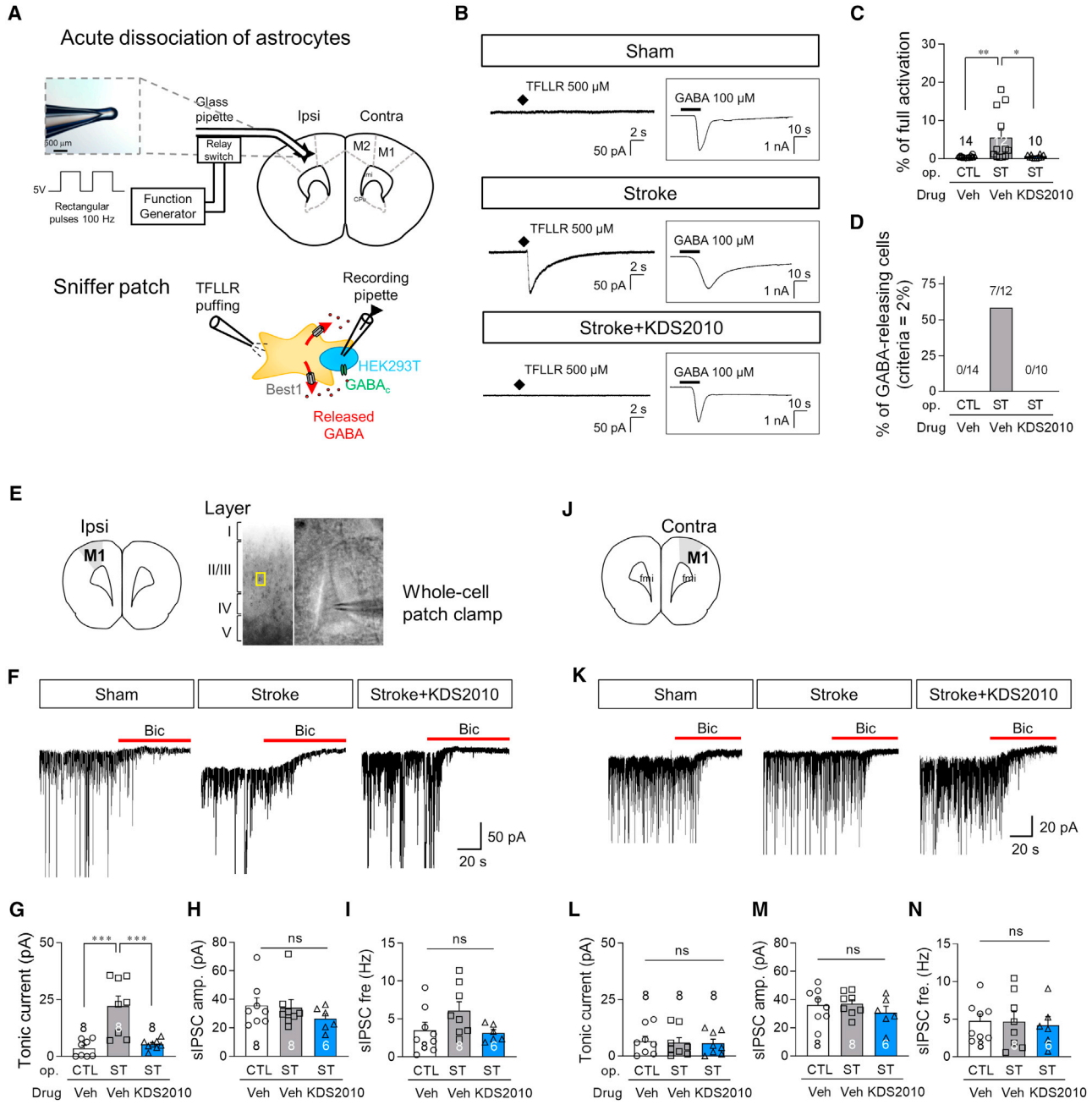

Figure 3. Pyramidal Neurons in Diaschisis Are Tonically Inhibited by Excessive Astrocytic GABA

(A) Schematic diagram of acute dissociation of astrocytes from motor cortex and sniffer patch.

(B) Representative traces of $GABA_CR$-mediated inward currents. Inset, GABA (100 μM)-induced inward currents (n = 3 for each group).

(C) Peak amplitudes of $GABA_CR$-mediated currents normalized to full activation ($F_{2, 33} = 6.849$, $p = 0.003$).

(D) Proportion of GABA-releasing astrocytes.

(E and J) Ipsilateral (E) or contralateral (J) motor cortex as ROIs and representative cell image of whole-cell patch clamp.

(F and K) Representative trace of $GABA_AR$-mediated currents (n = 3 for each group).

(G and L) Tonic GABA current (G, $F_{2, 21} = 14.34$, $p < 0.001$; L, $F_{2, 21} = 0.04737$, $p = 0.954$).

(H and M) Amplitude of sIPSC (H, $F_{2, 19} = 0.8124$, $p = 0.459$; M, $F_{2, 19} = 0.06969$, $p = 0.933$).

(I and N) Frequency of sIPSC (I, $F_{2, 19} = 2.519$, $p = 0.107$; N, $F_{2, 19} = 0.06894$, $p = 0.514$).

The number on each bar refers to the number of cells analyzed. N refers to the number of animals studied. For all panels, mean ± SEM, assessed using one-way ANOVA with Tukey test (*$p < 0.05$, **$p < 0.01$, and ***$p < 0.001$; ns, non-significant).

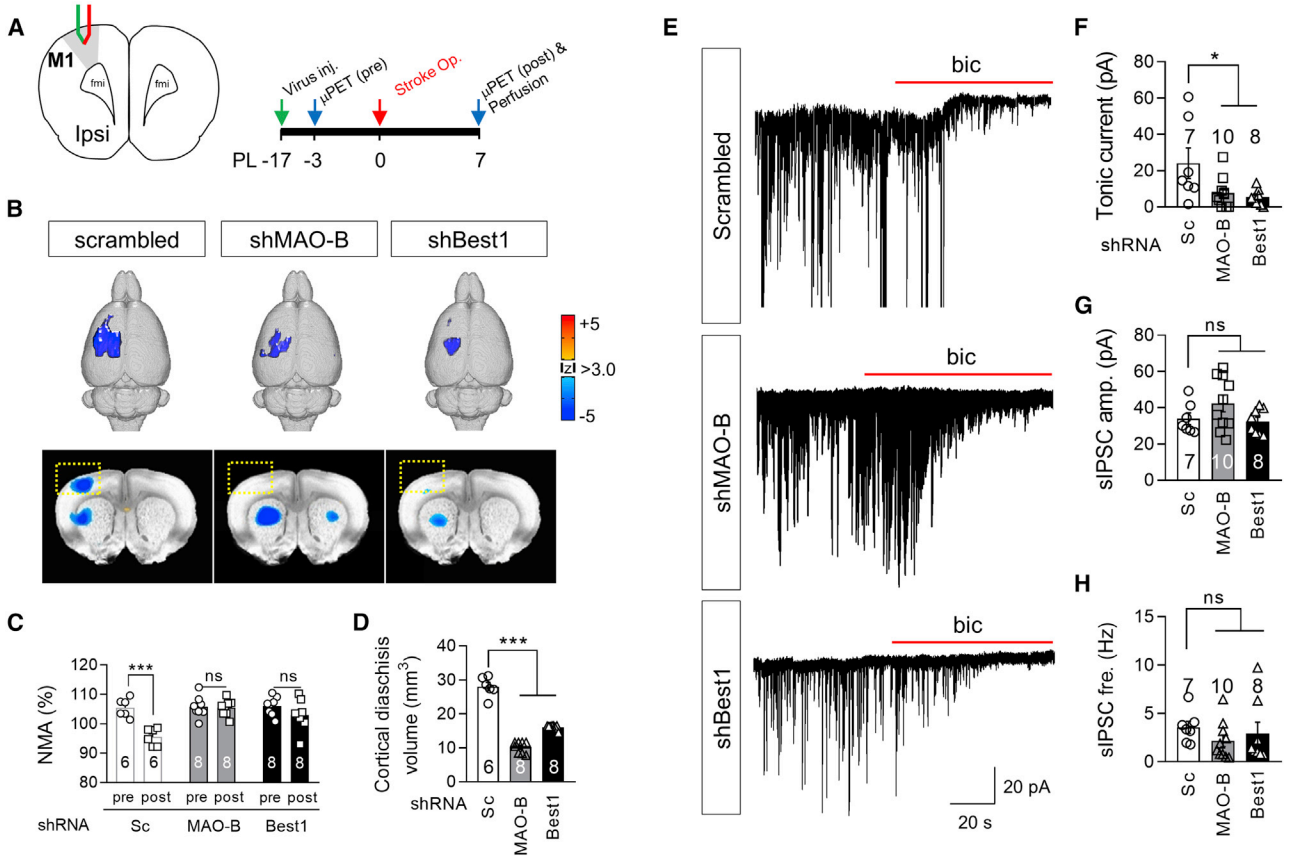

Figure 4. Astrocytic GABA Is Necessary for Diaschisis Formation

(A) Schematic diagram of virus injection and timeline of experiments.

(B) FDG-microPET images of scrambled-, MAO-B-shRNA-, or Best1-shRNA-injected stroke-operated rats.

(C) NMA changes after stroke operations ($F_{2, 19} = 10.20$, $p = 0.001$).

(D) Cortical diaschisis volume ($F_{2, 19} = 156.3$, $p < 0.001$).

(E) Representative traces of $GABA_AR$-mediated currents (n = 3, 3, and 4 for scrambled, MAO-B, and Best1-shRNA groups).

(F) Tonic GABA current ($F_{2, 22} = 4.552$, $p = 0.022$).

(G and H) Amplitude ($F_{2, 22} = 2.157$, $p = 0.140$) (G) and frequency ($F_{2, 22} = 0.7075$, $p = 0.5037$) (H) of sIPSC.

The number on each bar refers to the number of animals (C and D) or cells (F–H) analyzed. N refers to the number of animals studied. For all panels, mean ± SEM, assessed using RM two-way ANOVA with Bonferroni test (C) or one-way ANOVA with Dunnett test (F–H) (*$p < 0.05$, **$p < 0.01$, and ***$p < 0.001$; ns, non-significant).

attenuated the extent and volume of diaschisis (Figures 4B–4D) and excessive tonic GABA current (Figures 4E–4H). Taken together, our results indicate that MAO-B-dependent GABA, which is released through the Best1 channel from astrocytes, in the motor cortex is necessary for development of glucose hypometabolism.

We next tested if astrocytic GABA is sufficient to induce diaschisis-like glucose hypometabolism. Therefore, we aimed to determine whether reduction of metabolic rate can be caused by forcing astrocytic GABA synthesis by directly injecting putrescine, the precursor metabolite for GABA production in astrocytes (Figure 1F), into M1 (Figure S6A). We found that putrescine infusion significantly reduced metabolic rate on FDG-microPET (Figures S6B and S6C) and significantly increased astrocytic GABA and reactivity (Figures S6D–S6F). Furthermore, on the basis of previous reports that reactive astrocytes aberrantly synthesize GABA (Jo et al., 2014), we indirectly increased astrocytic GABA by injecting adeno-GFAP-GFP virus into the same brain region to induce astrogliosis (Figure 5A), as previously described (Woo et al., 2017). We observed marked glucose hypometabolism near the injection site (Figures 5B and 5C), with an appearance of numerous reactive astrocytes with increased GABA level (Figures 5D–5F), whereas saline injection induced neither reactive astrocytes nor hypometabolism. Next, we investigated whether MAO-B and tonic GABA are indeed critical for glucose hypometabolism with KDS2010 and L655,708. We orally treated the adenovirus-injected rats with KDS2010 for 7 days to block astrocytic GABA synthesis and found that the generation of glucose metabolic depression was significantly prevented by KDS2010 treatment (Figures 5G–5J), indicating the critical role of MAO-B in glucose hypometabolism. Unlike KDS2010, L655,708 was intraperitoneally administered only once to the

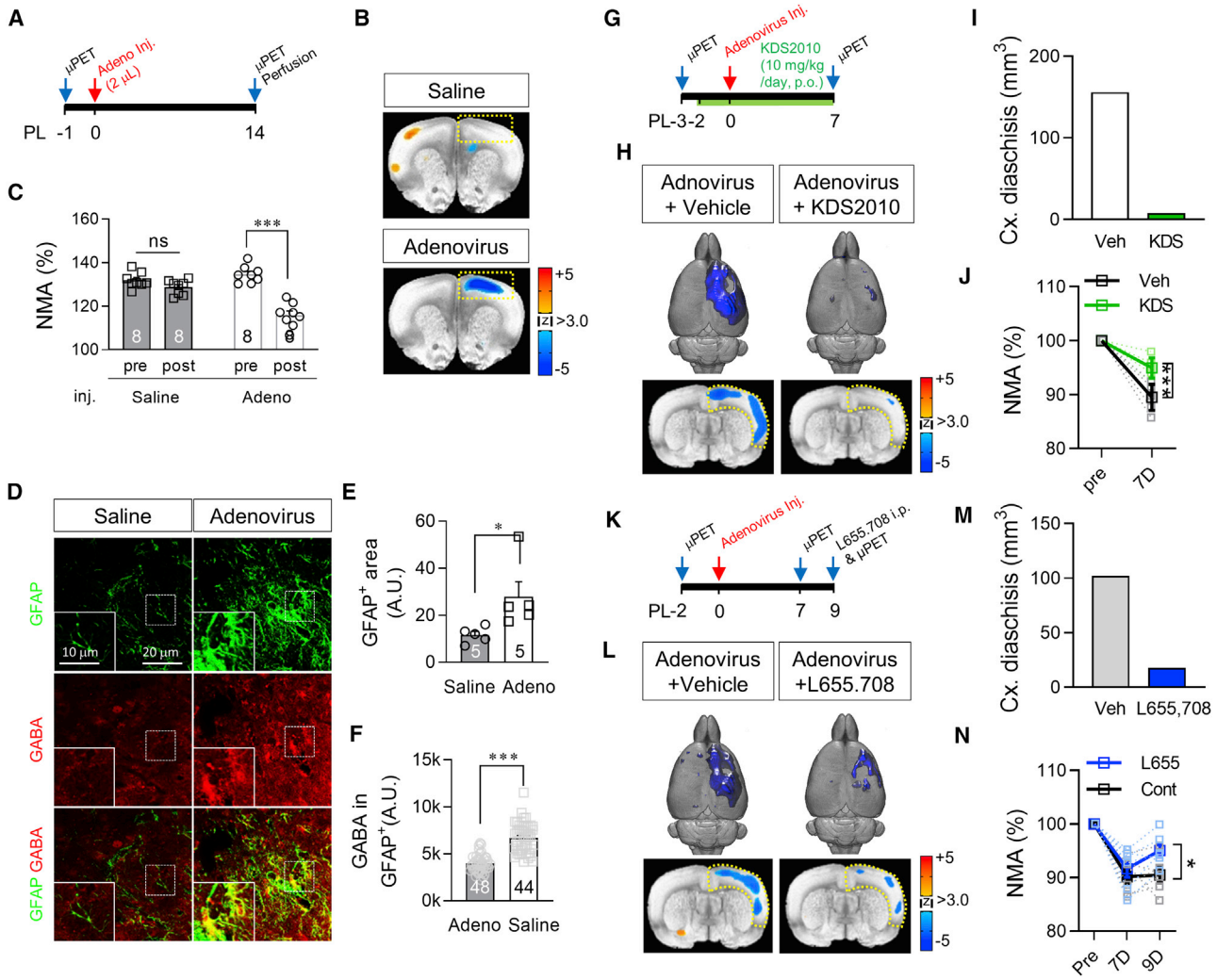

Figure 5. Astrocytic GABA Is Sufficient for Diaschisis-like Hypometabolism

(A) Timeline of adenovirus injection and microPET.

(B) FDG-microPET images after adeno-GFAP-GFP virus injection.

(C) NMA change ($F_{1, 14} = 42.04$, $p < 0.001$).

(D) Representative confocal images of GFAP, GABA, and NeuN (n = 5 for each group).

(E) GFAP-positive area ($t_8 = 2.406$, $p = 0.0427$; one image was analyzed from each animal).

(F) GABA intensity in GFAP-positive astrocytes ($t_{90} = 10.13$, $p < 0.001$).

(G and K) Timelines of experiments for treating adeno-GFAP-GFP virus-injected rats with KDS2010 (G) or L655,708 (K).

(H and L) FDG-microPET images with or without KDS2010 (H) or L655,708 treatment (L).

(I and M) Quantification of volume of cortex with glucose hypometabolism after KDS2010 treatment (I) or L655,708 treatment (M). KDS2010 inhibited the generation of glucose hypometabolism; L655,708 reversed the glucose hypometabolism.

(J and N) NMA change after adeno-GFAP-GFP virus injection with or without drug treatment (J, $F_{1, 10} = 18.94$, $p = 0.001$; N, $F_{2, 20} = 2.86$, $p = 0.081$).

The number on each bar refers to the number of animals (C), images (E), or cells (F) analyzed. N refers to the number of animals studied. For all panels, mean ± SEM, assessed using RM two-way ANOVA with Bonferroni test (C, J, and N) or two-tailed Student's t test (E and F) (*$p < 0.05$, **$p < 0.01$, and ***$p < 0.001$; ns, non-significant).

rats in which glucose hypometabolism was already confirmed, because the GABAARα5 inhibition can instantly block extrasynaptic GABA signaling. We found that glucose hypometabolism was also significantly reversed by L655,708 treatment (Figures 5K–5N), indicating the critical role of extrasynaptic GABA in glucose hypometabolism. Taken together, these findings indicate that MAO-B-mediated astrocytic GABA, which binds to extrasynaptic $GABA_AR\alpha5$ of neighboring neurons, is sufficient to induce diaschisis-like glucose hypometabolism.

Astrogliosis in the diaschisis region, which is distant from the original site of infarct in the internal capsule, could be attributed to retrograde atrophy of the motor neurons caused by massive collapse of axons of the corticospinal tract (Figure 1B). We confirmed the degenerative signs of soma, dendrites, and axons

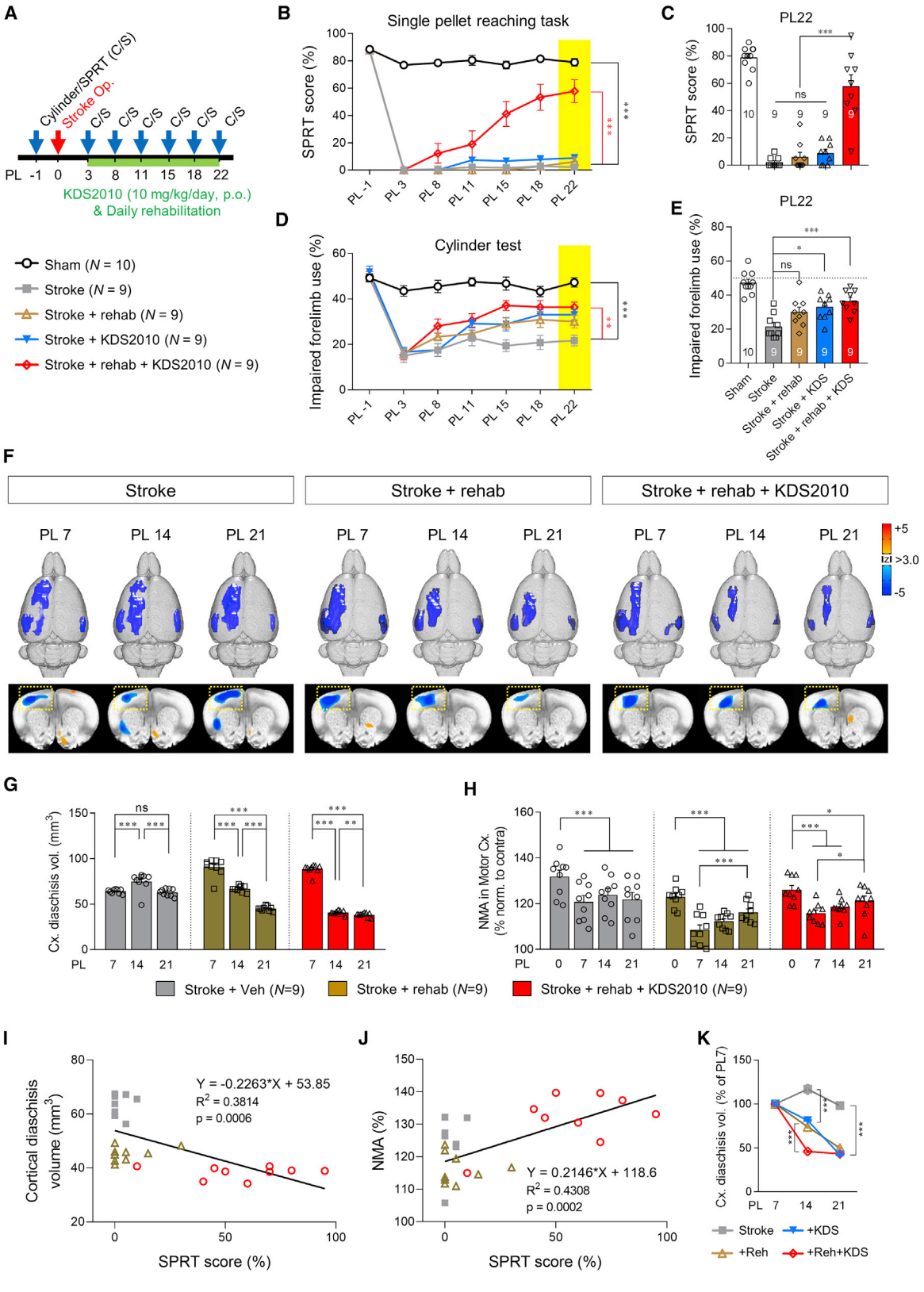

(legend on next page)

as well as decreased synapse numbers in the diaschisis region using electron microscopy (Figures S7A–S7F), without any alteration of the size of soma (Figures S7G–S7I). It is possible that this ultrastructural atrophy of damaged motor neurons is the cause of astrogliosis and aberrant astrocytic GABA synthesis, leading to tonic inhibition of the neighboring motor neurons and hypometabolism (Figure 7). This possibility needs to be validated in the future.

MAO-B Inhibition Facilitates Rehabilitation-Aided Post-stroke Recovery

A recent study showed that motor deficits following cortical stroke are mitigated by reducing $GABA_A$-mediated tonic inhibition (Clarkson et al., 2010), which we have revealed as the cause of the cortical hypometabolism in the capsular infarct model. Coincidently, the appearance of diaschisis is reported to be inversely correlated with recovery rate of stroke patients (Seitz et al., 1999; Takasawa et al., 2002). However, whether and how diaschisis contributes to post-stroke motor recovery from white matter stroke is unknown. To test if cortical hypometabolism in the diaschisis region impedes motor recovery following stroke, we treated the stroke-operated animals with KDS2010 and assessed the fine motor function of the contralesional forelimb by performing a single-pellet reaching task (SPRT) (Figure 6A). Contrary to our expectation, severe post-stroke motor deficits were not recovered by KDS2010 treatment alone (Figures 6B and 6C). A daily rehabilitation of 20 min SPRT training also did not recover motor function in this stroke model (Figures 6B and 6C), consistent with a previous study (Kim et al., 2016). Surprisingly, motor deficits were dramatically recovered when KDS2010 treatment was combined with rehabilitation (73% to sham group; Figures 6B and 6C). This trend was similarly observed in the cylinder test, which was used to assess general motor function (77% to sham group by combined treatment; Figures 6D and 6E). Consistent with behavioral recovery, we found that the combination of KDS2010 and rehabilitation significantly reduced cortical diaschisis volume and recovered reduced NMA (Figures 6F–6H). Diaschisis volume showed a significantly negative correlation with SPRT score (Figure 6I), while NMA showed a significantly positive correlation with SPRT score (Figure 6J). These findings indicate that the severity (i.e., extent and magnitude) of hypometabolism is tightly correlated with behavioral outcomes. Moreover, a lesion study with a high concentration (100 mM) of putrescine injection demonstrated that the brain region of glucose hypometabolism (i.e., motor cortex) is directly linked to motor function in the cylinder test and SPRT (Figures S6I–S6L). The most distinguishing feature of combined therapy was the faster reduction of diaschisis volume compared with rehabilitation or KDS2010 alone (Figure 6K). Taken together, reducing the severity of cortical hypometabolism by KDS2010 can significantly facilitate rehabilitation-aided functional recovery after stroke.

DISCUSSION

In this study, we have delineated the molecular and cellular mechanism of cortical hypometabolism in a subcortical stroke model and further established that reducing the astrocytic GABA synthesis by a reversible MAO-B inhibitor facilitates rehabilitation-aided motor recovery from stroke, providing a promising therapeutic strategy for post-stroke recovery. Our study highlights that a capsular infarct causes retrograde atrophy in the sensorimotor cortex, leading to a MAO-B-mediated excessive GABA production from reactive astrocytes (Figure 7). The tonic release of excessive GABA from reactive astrocytes via the Best1 channel strongly inhibits neighboring neuronal activity, which results in glucose hypometabolism (i.e., diaschisis). Furthermore, pharmacological blockade of astrocytic GABA synthesis significantly reduces the extent and volume of diaschisis and facilitates rehabilitation-aided functional recovery (Figure 7).

How can MAO-B inhibition cause functional recovery after white matter stroke? Astrocytic GABA-mediated diaschisis can exert a powerful brake on rehabilitation-mediated enhancement of neuronal activity, which could have induced a reorganization of recovery circuits. Indeed, we observed that combination therapy with rehabilitation and MAO-B inhibition caused a prominent and sustained increase in FDG signals in some subcortical structures, including medial thalamic nuclei, red nucleus, periaqueductal gray, and mesencephalic reticular formation, whereas rehabilitation alone or MAO-B inhibition caused only a marginal effect in those regions (Figure S1). These findings raise the possibility that combined therapy causes a reorganization of recovery circuits, which might participate in post-stroke recovery in the capsular stroke model (Figure 7). This exciting possibility awaits future investigations.

Overall, our findings are consistent with a previous clinical study demonstrating a possible beneficial effect of selegiline,

Figure 6. Combined Therapy of KDS2010 Treatment and Rehabilitation Recovers Post-stroke Motor Deficits

(A) Timeline of behavioral experiments and groups categorized by interventions.
(B) Schematic diagram of SPRT and SPRT score change by each intervention ($F_{24, 252} = 29.9$, $p < 0.001$).
(C) SPRT score at PL22 ($F_{4, 42} = 69.66$, $p < 0.001$).
(D) Left: schematic diagram of cylinder test. Right: ratio of impaired forelimb use assessed by cylinder test ($F_{24, 252} = 6.956$, $p < 0.001$).
(E) Ratio of impaired forelimb use at PL22 ($F_{4, 42} = 16.35$, $p < 0.001$).
(F) FDG-microPET images of sham, stroke, and stroke with KDS2010 treatment.
(G) Quantification of cortical diaschisis volume ($F_{4, 48} = 120.0$, $p < 0.001$).
(H) Time-dependent change of NMA in motor cortex ($F_{6, 72} = 2.101$, $p = 0.064$).
(I) Negative correlation between cortical diaschisis volume and SPRT score ($F_{1, 25} = 15.42$).
(J) Positive correlation between NMA of diaschisis region and SPRT score ($F_{1, 25} = 18.92$).
(K) Time-dependent change of normalized cortical diaschisis volume ($F_{6, 64} = 82.83$, $p < 0.001$).
The number on each bar refers to the number of animals analyzed. N refers to the number of animals studied. For all panels, mean ± SEM, assessed using one-way ANOVA with Tukey test (C and E) or RM two-way ANOVA with Bonferroni test (all other panels) (*$p < 0.05$, **$p < 0.01$, and ***$p < 0.001$; ns, non-significant).

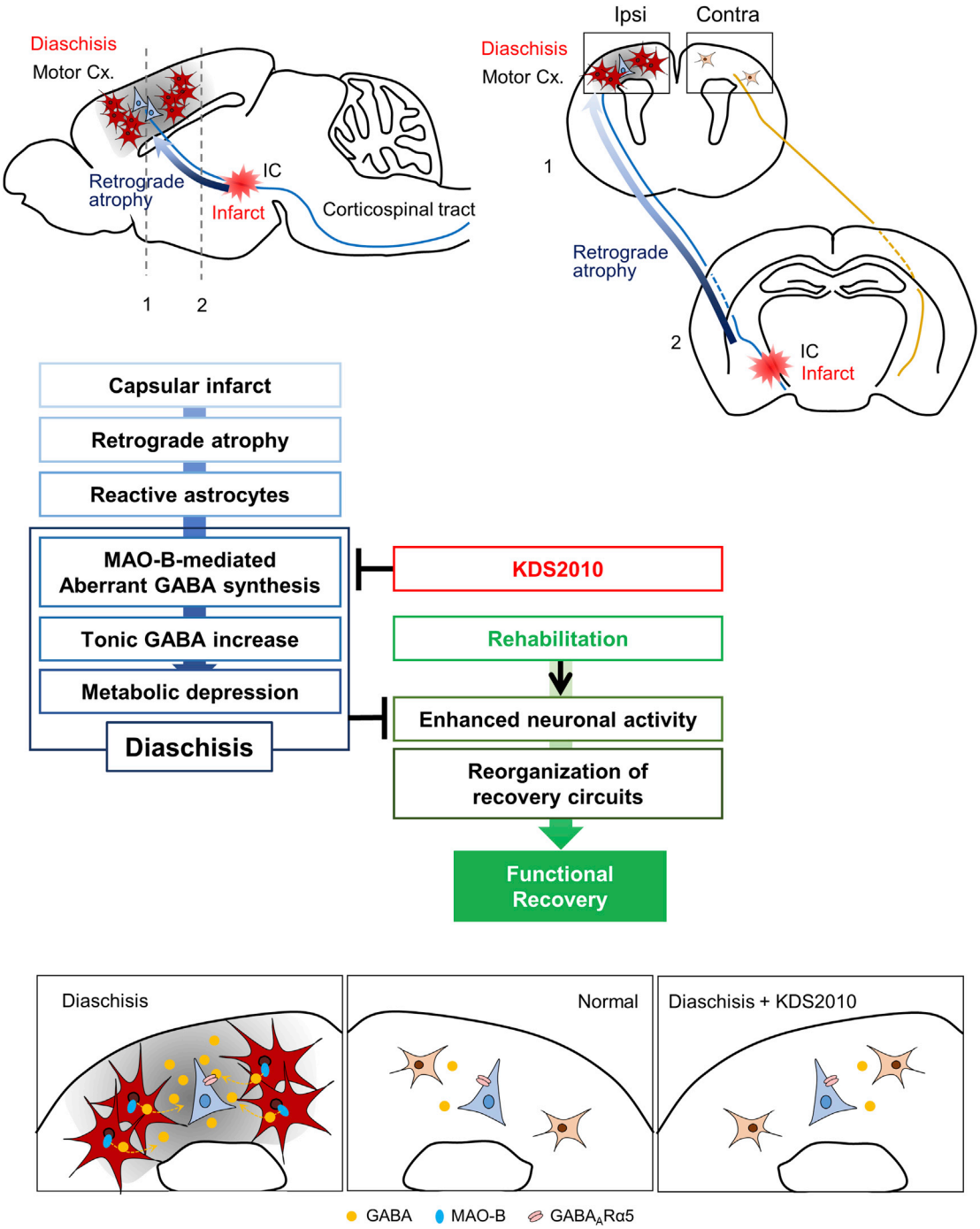

Figure 7. Schematic Diagram of Mechanism of Diaschisis through Excessive Tonic Inhibition Mediated by Astrocytic GABA and the Therapeutic Mechanism of Combination of KDS2010 and Rehabilitation

an irreversible MAO-B inhibitor, on recovery after stroke (Sivenius et al., 2001). However, in that study, the therapeutic effect of selegiline did not reach statistical significance (Sivenius et al., 2001). This is most likely due to the short-lived action of selegiline (Jo et al., 2014). Very recently, we demonstrated that prolonged treatment with selegiline fails to reduce aberrant astrocytic GABA because of compensatory upregulation of alternative GABA-synthetic enzymes in astrocytes, which could be attributed to the irreversibility of selegiline (Park et al., 2019). To overcome the shortcomings of irreversible MAO-B inhibitors such as selegiline, we have recently developed KDS2010, with high selectivity over MAO-A and reversibility with no significant

toxicity (Park et al., 2019). Our present study suggests KDS2010 as an effective replacement of selegiline for treatment of capsular stroke. Furthermore, KDS2010 is proved to possess an excellent pharmacokinetic profile, with high bioavailability (>100%), high blood-brain barrier permeability, and high target specificity in the central nervous system (Park et al., 2019). On the basis of these superior drug-like properties, pharmacological profiles, and potent therapeutic effect in the capsular infarct model, we propose KDS2010 as a next-generation drug candidate for capsular stroke.

In addition to producing GABA in astrocytes, MAO-B has long been believed to degrade dopamine and produce hydrogen peroxide. Therefore, the effect of KDS2010 on relieving diaschisis and post-stroke functional recovery in capsular infarct model might be attributed to inhibiting dopamine degradation, hydrogen peroxide production, and/or astrocytic GABA synthesis. In terms of dopamine degradation, numerous reports have suggested that the role of MAO-B in dopamine degradation has been exaggerated and have cast doubt on the role of MAO-B in dopamine degradation. For example, several studies demonstrated no change in extracellular dopamine level in MAO-B-deficient mice (Fornai et al., 1999) and selegiline-treated mice (Lamensdorf et al., 1996). These reports raise the possibility that MAO-A is more likely to be engaged in dopamine degradation than MAO-B. On the other hand, MAO-B is also well known as a producer of hydrogen peroxide, and MAO-B inhibition can reduce oxidative stress, raising the possibility that the therapeutic effect of KDS2010 could be attributed to a reduction of oxidative stress. However, we have demonstrated that the diaschisis is reversed by a treatment with L655,708, an inverse agonist of $GABA_AR\alpha5$, suggesting that KDS2010's effect is more likely due to MAO-B's action on GABA production rather than H_2O_2 production. Our findings suggest that MAO-B-dependent astrocytic GABA is the key molecule for the generation and maintenance of the diaschisis. On the other hand, we cannot completely rule out the possibility that functional recovery after stroke by KDS2010 is due to a reduction of MAO-B-dependent oxidative stress. This remaining possibility awaits further investigations.

The role of reactive astrocytes in the excitation/inhibition (E/I) balance has been controversial. Several studies have demonstrated that reactive astrocytes exhibit impaired function of glutamate uptake, causing neuronal hyperexcitability and spontaneous epileptic seizures (Ortinski et al., 2010; Robel et al., 2015). On the other hand, reactive astrocytes have been demonstrated to produce and release aberrantly excessive GABA to strongly inhibit neuronal excitability (Chun et al., 2018; Jo et al., 2014; Kim et al., 2017; Park et al., 2019; Wu et al., 2014). Reactive astrocytes might exhibit either of the two paradoxical characteristics or both, depending on the degree of reactivity, brain regions, or disease-specific local environment. We propose that astrogliosis in the epileptic brain and reactive astrocytes in the diaschisis region or in the Alzheimer's disease brain are distinct: the former might exhibit impaired glutamate uptake but less increased GABA production, while the latter might exhibit a greater increase in GABA production but less impaired glutamate uptake. Such a difference in glutamate uptake and GABA production should differentially affect the E/I balance. In the present study of a capsular stroke model, astrocytes in the motor cortex became reactive and exhibited a greater increase in GABA production, causing neuronal metabolic depression rather than neuronal hyperactivity.

Diaschisis, manifested by depression of blood flow and metabolism in a distant area following a focal brain injury, has been previously proposed as a prognostic marker for the likelihood of functional recovery in stroke patients (Takasawa et al., 2002). However, this proposal has not been properly validated. Our study provides the mechanistic insights for the proposed use of diaschisis-induced regional metabolic depression as a prognostic marker for functional recovery after capsular stroke. This was evidenced by the observed negative correlation between the extent of diaschisis-induced glucose hypometabolism and post-stroke functional recovery (Figure 7I). More important, we provide a potent therapeutic tool to actively reduce the extent of diaschisis, thus facilitating functional recovery after stroke. We hope that our therapeutic strategy of MAO-B inhibition by reversible MAO-B inhibitors for post-stroke recovery will be translated into clinical trials in the near future.

STAR★METHODS

Detailed methods are provided in the online version of this paper and include the following:

- KEY RESOURCES TABLE
- RESOURCE AVAILABILITY
  - Lead Contact
  - Materials Availability
  - Data and Code Availability
- EXPERIMENTAL MODEL AND SUBJECT DETAILS
- METHOD DETAILS
  - Photothrombotic capsular infarction
  - MicroPET Image acquisition and processing
  - Histological examination
  - Sniffer patch with acutely dissociated astrocytes
  - Flow Cytometry with acutely dissociated astrocytes
  - Astrocyte phenotyping
  - Calcium flux measurement
  - Whole-cell patch-clamp
  - Electron microcopy and toluidine blue staining
  - Drug administration
  - Measurements of MAO-B enzyme activity
  - Behavioral testing
  - Preparation and injection of putrescine and viruses
  - Quantitative real-time RT-PCR
- QUANTIFICATION AND STATISTICAL ANALYSIS
  - Image quantification
  - Statistical analyses

SUPPLEMENTAL INFORMATION

Supplemental Information can be found online at https://doi.org/10.1016/j.celrep.2020.107861.

ACKNOWLEDGMENTS

This work is supported by the Creative Research Initiative Program (2015R1A3A2066619) funded by National Research Foundation (NRF) of

Korea and Institute for Basic Science (IBS), Center for Cognition and Sociality (IBS-R001-D2) to C.J.L.; Basic Science Research Program funded by NRF of Korea (NRF-2016R1A2B3009660) and Biomedical Integrated Technology Research Project through a grant provided by GIST in 2017 to H.-I.K.; and KIST institutional program (Project No. 2E30180) through Korea Institute of Science and Technology funded by the Ministry of Science and ICT of Korea to M.-H.N.

AUTHOR CONTRIBUTIONS

H.-I.K., C.J.L., M.Y., and M.-H.N. conceived and designed the research. J.-Y.P., R.G.K., and H.S. performed surgical procedures. J.C., D.-H.K, S.L., and H.K. performed PET. M.-H.N., J.L., and W.W. performed immunohistochemistry. M.-H.N., J.W., and S.-J.O. performed electrophysiology. J.W.C., E.K.P., and K.D.P. synthesized the chemicals. H.-S.K. and M.-C.L. performed electron microscopy. H.J. and W.W. performed fluorescence-activated cell sorting. M.-H.N., J.C., H.-I.K., and C.J.L. wrote the manuscript. All authors provided ongoing critical review of results and commented on the manuscript.

DECLARATION OF INTERESTS

M.-H.N., J.C., J.-Y.P., S.-J.O., K.D.P., C.J.L., and H.-I.K. have a registered patent in the Republic of Korea on the therapeutic potential of KDS2010 for post-stroke recovery (KR-10-2005019) and the competing interests for the commercial development of KDS2010.

Received: July 18, 2019
Revised: May 18, 2020
Accepted: June 12, 2020
Published: July 7, 2020

REFERENCES

Badan, I., Buchhold, B., Hamm, A., Gratz, M., Walker, L.C., Platt, D., Kessler, Ch., and Popa-Wagner, A. (2003). Accelerated glial reactivity to stroke in aged rats correlates with reduced functional recovery. J. Cereb. Blood Flow Metab. *23*, 845–854.

Batiuk, M.Y., Martirosyan, A., Wahis, J., de Vin, F., Marneffe, C., Kusserow, C., Koeppen, J., Viana, J.F., Oliveira, J.F., Voet, T., et al. (2020). Identification of region-specific astrocyte subtypes at single cell resolution. Nat. Commun. *11*, 1220.

Bayraktar, O.A., Bartels, T., Holmqvist, S., Kleshchevnikov, V., Martirosyan, A., Polioudakis, D., Ben Haim, L., Young, A.M.H., Batiuk, M.Y., Prakash, K., et al. (2020). Astrocyte layers in the mammalian cerebral cortex revealed by a single-cell in situ transcriptomic map. Nat. Neurosci. *23*, 500–509.

Bi, F., Huang, C., Tong, J., Qiu, G., Huang, B., Wu, Q., Li, F., Xu, Z., Bowser, R., Xia, X.G., and Zhou, H. (2013). Reactive astrocytes secrete lcn2 to promote neuron death. Proc. Natl. Acad. Sci. U S A *110*, 4069–4074.

Burda, J.E., and Sofroniew, M.V. (2014). Reactive gliosis and the multicellular response to CNS damage and disease. Neuron *81*, 229–248.

Carrera, E., and Tononi, G. (2014). Diaschisis: past, present, future. Brain *137*, 2408–2422.

Chu, W.J., Mason, G.F., Pan, J.W., Hetherington, H.P., Liu, H.G., San Pedro, E.C., and Mountz, J.M. (2002). Regional cerebral blood flow and magnetic resonance spectroscopic imaging findings in diaschisis from stroke. Stroke *33*, 1243–1248.

Chun, H., An, H., Lim, J., Woo, J., Lee, J., Ryu, H., and Lee, C.J. (2018). Astrocytic proBDNF and tonic GABA distinguish active versus reactive astrocytes in hippocampus. Exp. Neurobiol. *27*, 155–170.

Clarkson, A.N., Huang, B.S., Macisaac, S.E., Mody, I., and Carmichael, S.T. (2010). Reducing excessive GABA-mediated tonic inhibition promotes functional recovery after stroke. Nature *468*, 305–309.

Cox, R.W. (1996). AFNI: software for analysis and visualization of functional magnetic resonance neuroimages. Comput. Biomed. Res. *29*, 162–173.

Endoh, M., Maiese, K., and Wagner, J. (1994). Expression of the inducible form of nitric oxide synthase by reactive astrocytes after transient global ischemia. Brain Res. *651*, 92–100.

Finger, S., Koehler, P.J., and Jagella, C. (2004). The Monakow concept of diaschisis: origins and perspectives. Arch. Neurol. *61*, 283–288.

Fornai, F., Chen, K., Giorgi, F.S., Gesi, M., Alessandri, M.G., and Shih, J.C. (1999). Striatal dopamine metabolism in monoamine oxidase B-deficient mice: a brain dialysis study. J. Neurochem. *73*, 2434–2440.

Garbuzova-Davis, S., Rodrigues, M.C., Hernandez-Ontiveros, D.G., Tajiri, N., Frisina-Deyo, A., Boffeli, S.M., Abraham, J.V., Pabon, M., Wagner, A., Ishikawa, H., et al. (2013). Blood-brain barrier alterations provide evidence of subacute diaschisis in an ischemic stroke rat model. PLoS ONE *8*, e63553.

Gharbawie, O.A., Gonzalez, C.L., and Whishaw, I.Q. (2005). Skilled reaching impairments from the lateral frontal cortex component of middle cerebral artery stroke: a qualitative and quantitative comparison to focal motor cortex lesions in rats. Behav. Brain Res. *156*, 125–137.

Heo, J.Y., Nam, M.H., Yoon, H.H., Kim, J., Hwang, Y.J., Won, W., Woo, D.H., Lee, J.A., Park, H.J., Jo, S., et al. (2020). Aberrant tonic inhibition of dopaminergic neuronal activity causes motor symptoms in animal models of Parkinson's disease. Curr. Biol. *30*, 276–291.e9.

Hsu, J.E., and Jones, T.A. (2005). Time-sensitive enhancement of motor learning with the less-affected forelimb after unilateral sensorimotor cortex lesions in rats. Eur. J. Neurosci. *22*, 2069–2080.

Hua, Y., Schallert, T., Keep, R.F., Wu, J., Hoff, J.T., and Xi, G. (2002). Behavioral tests after intracerebral hemorrhage in the rat. Stroke *33*, 2478–2484.

Jo, S., Yarishkin, O., Hwang, Y.J., Chun, Y.E., Park, M., Woo, D.H., Bae, J.Y., Kim, T., Lee, J., Chun, H., et al. (2014). GABA from reactive astrocytes impairs memory in mouse models of Alzheimer's disease. Nat. Med. *20*, 886–896.

Kim, H.S., Kim, D., Kim, R.G., Kim, J.M., Chung, E., Neto, P.R., Lee, M.C., and Kim, H.I. (2014). A rat model of photothrombotic capsular infarct with a marked motor deficit: a behavioral, histologic, and microPET study. J. Cereb. Blood Flow Metab. *34*, 683–689.

Kim, D., Kim, R.G., Kim, H.S., Kim, J.M., Jun, S.C., Lee, B., Jo, H.J., Neto, P.R., Lee, M.C., and Kim, H.I. (2015). Longitudinal changes in resting-state brain activity in a capsular infarct model. J. Cereb. Blood Flow Metab. *35*, 882.

Kim, R.G., Cho, J., Ree, J., Kim, H.S., Rosa-Neto, P., Kim, J.M., Lee, M.C., and Kim, H.I. (2016). Sensory-parietal cortical stimulation improves motor recovery in severe capsular infarct. J. Cereb. Blood Flow Metab. *36*, 2211–2222.

Kim, Y.S., Woo, J., Lee, C.J., and Yoon, B.E. (2017). Decreased glial GABA and tonic inhibition in cerebellum of mouse model for attention-deficit/hyperactivity disorder (ADHD). Exp. Neurobiol. *26*, 206–212.

Lalo, U., Pankratov, Y., Kirchhoff, F., North, R.A., and Verkhratsky, A. (2006). NMDA receptors mediate neuron-to-glia signaling in mouse cortical astrocytes. J. Neurosci. *26*, 2673–2683.

Lalo, U., Palygin, O., North, R.A., Verkhratsky, A., and Pankratov, Y. (2011). Age-dependent remodelling of ionotropic signalling in cortical astroglia. Aging Cell *10*, 392–402.

Lalo, U., Palygin, O., Rasooli-Nejad, S., Andrew, J., Haydon, P.G., and Pankratov, Y. (2014). Exocytosis of ATP from astrocytes modulates phasic and tonic inhibition in the neocortex. PLoS Biol. *12*, e1001747.

Lamensdorf, I., Youdim, M.B., and Finberg, J.P. (1996). Effect of long-term treatment with selective monoamine oxidase A and B inhibitors on dopamine release from rat striatum in vivo. J. Neurochem. *67*, 1532–1539.

Lee, C.J., Mannaioni, G., Yuan, H., Woo, D.H., Gingrich, M.B., and Traynelis, S.F. (2007). Astrocytic control of synaptic NMDA receptors. J. Physiol. *581*, 1057–1081.

Lee, Y., Messing, A., Su, M., and Brenner, M. (2008). GFAP promoter elements required for region-specific and astrocyte-specific expression. Glia *56*, 481–493.

Lee, S., Yoon, B.E., Berglund, K., Oh, S.J., Park, H., Shin, H.S., Augustine, G.J., and Lee, C.J. (2010). Channel-mediated tonic GABA release from glia. Science *330*, 790–796.

Li, Y., Wang, D., Zhang, H., Wang, Y., Wu, P., Zhang, H., Yang, Y., and Huang, W. (2016). Changes of brain connectivity in the primary motor cortex after subcortical stroke: a multimodal magnetic resonance imaging study. Medicine (Baltimore) *95*, e2579.

Lundgaard, I., Li, B., Xie, L., Kang, H., Sanggaard, S., Haswell, J.D., Sun, W., Goldman, S., Blekot, S., Nielsen, M., et al. (2015). Direct neuronal glucose uptake heralds activity-dependent increases in cerebral metabolism. Nat. Commun. *6*, 6807.

Mucke, L., and Eddleston, M. (1993). Astrocytes in infectious and immune-mediated diseases of the central nervous system. FASEB J. *7*, 1226–1232.

Oh, S.J., and Lee, C.J. (2017). Distribution and function of the Bestrophin-1 (Best1) channel in the brain. Exp. Neurobiol. *26*, 113–121.

Ortinski, P.I., Dong, J., Mungenast, A., Yue, C., Takano, H., Watson, D.J., Haydon, P.G., and Coulter, D.A. (2010). Selective induction of astrocytic gliosis generates deficits in neuronal inhibition. Nat. Neurosci. *13*, 584–591.

Pandit, S., Neupane, C., Woo, J., Sharma, R., Nam, M.H., Lee, G.S., Yi, M.H., Shin, N., Kim, D.W., Cho, H., et al. (2020). Bestrophin1-mediated tonic GABA release from reactive astrocytes prevents the development of seizure-prone network in kainate-injected hippocampi. Glia *68*, 1065–1080.

Papp, E.A., Leergaard, T.B., Calabrese, E., Johnson, G.A., and Bjaalie, J.G. (2014). Waxholm space atlas of the Sprague Dawley rat brain. Neuroimage *97*, 374–386.

Park, J.-H., Ju, Y., Choi, J.W., Song, H.J., Jang, B.K., Woo, J., Chun, H., Kim, H.J., Shin, S.J., Yarishkin, O., et al. (2019). Newly developed reversible MAO-B inhibitor circumvents the shortcomings of irreversible inhibitors in Alzheimer's disease. Sci. Adv. *5*, eaav0316.

Robel, S., Buckingham, S.C., Boni, J.L., Campbell, S.L., Danbolt, N.C., Riedemann, T., Sutor, B., and Sontheimer, H. (2015). Reactive astrogliosis causes the development of spontaneous seizures. J. Neurosci. *35*, 3330–3345.

Sacco, S., Marini, C., Totaro, R., Russo, T., Cerone, D., and Carolei, A. (2006). A population-based study of the incidence and prognosis of lacunar stroke. Neurology *66*, 1335–1338.

Seitz, R.J., Azari, N.P., Knorr, U., Binkofski, F., Herzog, H., and Freund, H.J. (1999). The role of diaschisis in stroke recovery. Stroke *30*, 1844–1850.

Shim, H.S., Park, H.J., Woo, J., Lee, C.J., and Shim, I. (2019). Role of astrocytic GABAergic system on inflammatory cytokine-induced anxiety-like behavior. Neuropharmacology *160*, 107776.

Sivenius, J., Sarasoja, T., Aaltonen, H., Heinonen, E., Kilkku, O., and Reinikainen, K. (2001). Selegiline treatment facilitates recovery after stroke. Neurorehabil. Neural Repair *15*, 183–190.

Song, H., Park, J.Y., Kim, H.S., Lee, M.C., Kim, Y., and Kim, H.I. (2016). Circumscribed capsular infarct modeling using a photothrombotic technique. J. Vis. Exp. (*112*), 53281.

Song, H., Jung, W., Lee, E., Park, J.Y., Kim, M.S., Lee, M.C., and Kim, H.I. (2017). Capsular stroke modeling based on somatotopic mapping of motor fibers. J. Cereb. Blood Flow Metab. *37*, 2928–2937.

Takasawa, M., Watanabe, M., Yamamoto, S., Hoshi, T., Sasaki, T., Hashikawa, K., Matsumoto, M., and Kinoshita, N. (2002). Prognostic value of subacute crossed cerebellar diaschisis: single-photon emission CT study in patients with middle cerebral artery territory infarct. AJNR Am. J. Neuroradiol. *23*, 189–193.

Tatsch, K., Koch, W., Linke, R., Poepperl, G., Peters, N., Holtmannspoetter, M., and Dichgans, M. (2003). Cortical hypometabolism and crossed cerebellar diaschisis suggest subcortically induced disconnection in CADASIL: an 18F-FDG PET study. J. Nucl. Med. *44*, 862–869.

Woo, J., Im, S.K., Chun, H., Jung, S.Y., Oh, S.J., Choi, N., Lee, C.J., and Hur, E.M. (2017). Functional characterization of resting and adenovirus-induced reactive astrocytes in three-dimensional culture. Exp. Neurobiol. *26*, 158–167.

Wu, Z., Guo, Z., Gearing, M., and Chen, G. (2014). Tonic inhibition in dentate gyrus impairs long-term potentiation and memory in an Alzheimer's [corrected] disease model. Nat. Commun. *5*, 4159.

Yamashita, Y., Wada, I., Horiba, M., and Sahashi, K. (2016). Influence of cerebral white matter lesions on the activities of daily living of older patients with mild stroke. Geriatr. Gerontol. Int. *16*, 942–947.

Yoon, B.E., Woo, J., Chun, Y.E., Chun, H., Jo, S., Bae, J.Y., An, H., Min, J.O., Oh, S.J., Han, K.S., et al. (2014). Glial GABA, synthesized by monoamine oxidase B, mediates tonic inhibition. J. Physiol. *592*, 4951–4968.

STAR★METHODS

KEY RESOURCES TABLE

REAGENT or RESOURCE	SOURCE	IDENTIFIER
Antibodies		
Chicken anti-GFAP	Millipore	Cat# ab5541; RRID: AB_177521
Mouse anti-Neurofilament	DAKO	Cat# M0762; RRID: AB_2314899
Guinea pig anti-GABA	Millipore	Cat# ab175; RRID: AB_91011
Mouse anti-NeuN	Millipore	Cat# MAB377; RRID: AB_2298772
Goat anti-Maob	Santa Cruz	Cat# sc-18401; RRID: AB_2137271
Rabbit anti-PV	Swant	Cat# PV27; RRID: AB_2631173
Goat anti-LCN2	Abcam	Cat# ab31289; RRID: AB_776042
Rabbit anti-Iba1	Wako	Cat# 019-19741; RRID: AB_839504
DAPI	Pierce	Cat# D1306; RRID: AB_2629482
Alexa 488 donkey anti-chicken	Jackson ImmunoResearch	Cat# 703-545-155, RRID: AB_2340375
Alexa-594 donkey anti-rabbit	Jackson ImmunoResearch	Cat# 711-585-152, RRID: AB_2340621
Alexa-647 donkey anti-mouse	Jackson ImmunoResearch	Cat# 715-605-151; RRID: AB_2340863
Alexa-594 donkey anti-guinea pig	Jackson ImmunoResearch	Cat# 706-585-148; RRID: AB_2340474
Alexa-647 donkey anti-rabbit	Jackson ImmunoResearch	Cat#; 711-605-152 RRID: AB_2492288
Bacterial and Virus Strains		
AAV_{DJ}-GFAP-Cre-mCherry	KIST virus facility	N/A
Lenti-pSico-MAOB-shRNA-GFP	KIST virus facility	N/A
Lenti-pSico-scrambled-shRNA-GFP	KIST virus facility	N/A
Adeno-GFAP-GFP	KIST virus facility	N/A
Chemicals, Peptides, and Recombinant Proteins		
KDS2010	This paper	N/A
Putrescine dihydrochloride	Sigma aldrich	Cat# P7075; CAS: 333-93-7
Rose Bengal	Sigma aldrich	Cat# 330000; CAS: 632-69-9
L655,708	Sigma aldrich	Cat# L9787; CAS: 130477-52-0
Amplex Red Monoamine oxidase Assay Kit	Invitrogen	Cat# A12214; CAS: N/A
GABA	Tocris	Cat# 0344; CAS: 56-12-2
D-AP5	Tocris	Cat# 0106; CAS: 79055-68-8
CNQX	Tocris	Cat# 0190; CAS: 115066-14-3
(-)-Bicuculline methobromide	Tocris	Cat# 0109; CAS: 73604-30-5
NO-711 hydrochloride	Sigma aldrich	Cat# N142; CAS: 145645-62-1
(S)-SNAP-5114	Sigma aldrich	Cat# S1069; CAS: 157604-55-2
Critical Commercial Assays		
Amplex Red Monoamine Oxidase Assay Kit	Thermo Fisher Scientific	Cat#: A12214
Experimental Models: Cell Lines		
Human: HEK293T cells	Korean Cell Line Bank (Seoul National University)	RRID:CVCL_0045
Experimental Models: Organisms/Strains		
Mouse: Sprague Dawley rats	Taconic	Cat# SD-M
Oligonucleotides		
MAOB shRNA targeting sequence: AAT CGT AAG ATA CGA TTC TGG	Jo et al., 2014	N/A
Recombinant DNA		
pSicoR-MAOBshRNA-mCherry	Jo et al., 2014	N/A
pSicoR-scrambled-shRNA-mCherry	Jo et al., 2014	N/A

(*Continued on next page*)

Continued

REAGENT or RESOURCE	SOURCE	IDENTIFIER
Software and Algorithms		
GraphPad Prism 7, 8	GraphPad software	https://www.megasoftware.net/home; RRID:SCR_005375
NIS-Elements	Nikon	https://www.nikonmetrology.com/en-gb/product/nis-elements-microscope-imaging-software
ImageJ program	NIH	https://imagej.nih.gov/ij/download.html
Minianalysis	Synaptosoft	http://www.synaptosoft.com/MiniAnalysis/

RESOURCE AVAILABILITY

Lead Contact

Further information and requests for resources and reagents should be directed to and will be fulfilled by the Lead Contact, C. Justin Lee (cjl@kist.re.kr).

Materials Availability

This study did not generate new unique reagents, plasmids, nor mouse lines.

Data and Code Availability

This study did not generate any code.

EXPERIMENTAL MODEL AND SUBJECT DETAILS

Animal care and handling were performed according to the directives of the Animal Care and Use Committee and institutional guidelines of KIST (Seoul, Korea) and GIST (Gwangju, Korea). Experiments were performed on 105 adult male Sprague Dawley rats (9 weeks old, ~300 g) including stroke experiment (N = 73) and cortex gliosis-inducing experiment (N = 32). All animals were housed two per cage in a controlled animal facility with *ad libitum* access to food and water. The animal care unit was maintained on a 12 h light–dark cycle (07:00 – 19:00) with controlled temperature (21 ± 1°C) and humidity (50%).

Forty-six rats underwent circumscribed photothrombotic stroke lesioning in the posterior limb of the internal capsule (PLIC) and were randomly allocated into 5 groups based on the rehabilitative training and administration of MAO-B inhibitor (KDS2010): (1) sham operated group (N = 10, **Sham**), (2) non-rehabilitation group without KDS2010 treatment (N = 9, **Stroke**), (3) non-rehabilitation group with KDS2010 (N = 9, **Stroke+KDS2010**), (4) rehabilitation group without KDS2010 (N = 9, **Stroke+rehab**), (5) rehabilitation group with KDS2010 (N = 9, **Stroke+rehab+KDS2010**). The proportion of left-handed animals in each group was as follows: 40%, 44%, 33%, 33%, and 56% for sham, stroke, stroke+rehab, stroke+KDS, and stroke+KDS+rehab, respectively. Twenty-two rats underwent lentivirus carrying MAO-B shRNA (N = 8), Best1-shRNA (N = 8) or scrambled shRNA injection (N = 6) into motor cortex and stroke lesioning in the PLIC. Thirty-two rats underwent adeno-GFAP-GFP virus injection (N = 8), saline-control (N = 8), or putrescine injection (N = 8), saline-control (N = 8). Eighteen rats underwent stroke lesioning in the PLIC and treated with KDS2010 (N = 6), L655,708 (N = 6), or saline (N = 6). Five rats underwent stroke lesioning in the PLIC and sacrificed for electrophysiology with GABA transporter (GAT) blockers (NO-711 and SNAP-5114). Fifteen rats were underwent stroke lesioning for RT-qPCR analysis including five sham-control animals. Ten rats were underwent cortical lesioning with putrescine (100 mM) including five sham-control animals.

METHOD DETAILS

Photothrombotic capsular infarction

Rats underwent photothrombotic capsular stroke lesioning in the PLIC as previously described (Kim et al., 2014; Song et al., 2016). Briefly, animals were anesthetized with a mixture of ketamine hydrochloride (100 mg/kg) and xylazine (7 mg/kg) and rectal temperature was maintained at 37 ± 0.5°C using heating pad. The optic fiber with a core diameter of 62.5 μm and an outer diameter of 125 μm was stereotaxically inserted into PLIC target (AP = −2.0 mm, ML = 3.1 mm from bregma, DV = 7.2 mm from dura). Rose Bengal dye (20 mg/kg) was injected through the tail vein. Then, the target was irradiated for 1.5 minutes using the green laser (3.7mW). After laser irradiation, the optical fiber was removed and the scalp wound was sutured. After surgery, the animal was treated with ketoprofen (2 mg/kg, i.m.) for pain control. The sham group underwent the same surgical procedure, except that they received an injection of 0.9% saline instead of Rose Bengal dye.

The stroke operation was validated by the first set of SPRT which was performed 3 days after stroke operation. Normally, the stroke-operated rats show distinctively impaired motor behavior, while 20%–30% of the rats did not, which is due to improper targeting of light fiber during stroke operation. These animals, which did not show impaired motor behavior 3 days after stroke operation, were dropped in the following experiments. No animal was excluded from the analysis after behavioral experiments and FDG-microPET scanning.

MicroPET Image acquisition and processing

Longitudinal microPET scans were performed to measure the regional glucose metabolism before and after lesioning, administration of KDS2010, and rehabilitative training. Each rat was scanned a total of four times: a baseline scan prior to infarct lesioning (PL −1), and scans on post-lesion (PL) days 7, 14, and 21. The microPET/CT scanner (Inveon, Siemens Medical Solution) has a transaxial resolution of 1.4 mm full width at half maximum and a 12.7 mm field of view. Animals were food-deprived for 12 h before each scan, and 2-deoxy-2-[^{18}F]-fluoro-D-glucose (FDG; 0.1 mCi/100 g) was injected into the tail vein. After a 30-minute uptake period, the animals were anesthetized with 2% isoflurane and transferred in the scanner. The head was fixed with a customized head holder (Hyosung Inc.). Vital signs including respiration (50 ± 5 respirations/min), heart rate (280 ± 20 beats/min), and rectal temperature (37.0 ± 1°C) were monitored during scanning procedures (BioVet, m2m Imaging Corp). A 25-min static acquisition and 5-min attenuation-correction computed tomography scan were performed. The acquired images were reconstructed with the iterative OSEM3D/MAP algorithm. Image analysis was performed with the Analysis of Functional NeuroImages (AFNI) package (Cox, 1996). All acquired images were automatically co-registered to the MRI template of Sprague Dawley rat brain (Papp et al., 2014), and manual co-registration was performed for minor misalignment to the template. Images were normalized to the mean value of the whole brain and spatially smoothed using a 3-D isotropic Gaussian kernel with 1.2 mm full width at half maximum. MRIcroGL program was used to acquire the 3-D rendered images (http://www.cabiatl.com/mricrogl/).

To identify the metabolic activity of a specific brain region, we utilized NMA (normalized metabolic activity) which is each voxel's standardized uptake value (SUV) of FDG normalized by averaged SUV throughout the whole brain. SUV is the quantity of incorporated FDG in a specific brain region of each animal.

In addition, microPET scans were performed in the same way for cortex gliosis-inducing experiment. Each rat was scanned twice: pre-injection and post-injection scans (AAV and putrescine). For AAV injection group, the post-injection scan was done after 2 weeks of injection, in contrast, the putrescine-injection group was scanned after 2 days. Eight rats which received the injection of saline instead of AAV or Putrescine and scans were used for control.

For investigating the effect of KDS2010 and L655,708 in adeno-GFAP-GFP-induced decrease in FDG uptake, we also performed microPET scans. For KDS2010 experiment, each rat was scanned twice: pre-injection (3 days prior to virus injection) and post-injection scans (7 days after virus injection). For L655,708 experiment, each rat was scanned three times: pre-injection (3 days prior to virus injection), pre-L655,708 (7 days after virus injection), and post-L655,708 (9 days after virus injection). Scanning and analyses were performed in a same way as described above.

Histological examination

For immunohistochemistry, animals were anaesthetized with ketamine (100 mg/kg), and perfused transcardially with 0.9% saline solution followed by 4% paraformaldehyde in 0.1 M phosphate buffered saline (PBS). After post-fixation with 4% paraformaldehyde for 12 h and cryoprotection with 30% sucrose, the brains were coronally sectioned with 30-μm thickness. Sections were stained for hematoxylin and eosin (H&E), and immunostained for GFAP, neurofilament-M/H, or Iba1 protein. Primary antibodies were used as follow: GFAP (1:400, Invitrogen, PA1-9565) and neurofilament (1:600, Dako, M0762). Immunostaining was performed using the avidin-biotin peroxidase method with the ABC Kit (Vector Laboratories), as previously described (Woo et al., 2017). In brief, antigen retrieval was conducted by heating the tissue sections at 60°C for 5 minutes in sodium citrate buffer, after which the sections were incubated in a mixture of 3% hydrogen peroxide and 10% methanol for 20 minutes, followed by 10% goat serum for 1 h at room temperature. The sections were incubated with each primary antibody for 2 h, biotinylated secondary antibody for 20 minutes, and streptavidin-horseradish peroxidase (Dako Cytomation) for 20 minutes. They were then developed with a chromogenic solution of diaminobenzidine and counterstained with hematoxylin to visualize cell nuclei. Known positive and negative tissues were used as controls.

For immunofluorescence, 30 μm-thick cryosections were incubated for 1 h in a blocking solution (0.3% Triton-X, 3% donkey serum in 0.1 M PBS) and then immunostained with a mixture of primary antibodies in a blocking solution at 4°C on a shaker overnight. After washing in PBS 3 times, sections were incubated with corresponding fluorescent secondary antibodies for 1.5 h and then washed with PBS 3 times. If needed, DAPI (Pierce, 1:3,000) was stained during the second washing step. Finally, sections were mounted with fluorescent mounting medium (Dako) and dried. A series of fluorescent images were obtained with A1 Nikon confocal microscope, and 30-μm Z stack images in 3-μm steps were processed for further analysis using NIS-Elements (Nikon) software and ImageJ (NIH) program. The primary antibodies used for fluorescent immunostaining were as follows: chicken anti-GFAP (1:500; Millipore ab5541), guinea pig anti-GABA (1:200; Millipore ab175), mouse anti-NeuN (1:1000; Millipore MAB377), goat anti-MAOB (1:100; Santa cruz sc-18401), rabbit anti-PV (1:500; Swant PV27), goat anti-LCN2 (1:50; Abcam ab31289), and rabbit anti-Iba1 (1:200; Wako 019-19741). Fluorescent secondary antibodies were purchased from Invitrogen or Jackson ImmunoResearch and used in 1:500 dilutions.

Sniffer patch with acutely dissociated astrocytes

Sniffer patch was performed as described with a slight modification (Jo et al., 2014). The quickly excised brain was submerged in ice-cold cutting solution that contained (in mM): 250 sucrose, 26 $NaHCO_3$, 10 d-(+)-glucose, 4 $MgCl_2$, 3 myo-inositol, 2.5 KCl, 2 sodium pyruvate, 1.25 NaH_2PO_4, 0.5 ascorbic acid, 0.1 $CaCl_2$ and 1 kynurenic acid, pH 7.4. All solution was gassed with 95% O2 – 5% CO2. The brain regions containing motor cortex including diaschisis region were coronally sliced in 300 μm-thickness using a vibrating microtome (VT1000S, Leica). The motor cortical region of each slice was mechanically dissociated with a round-tip of vibrating polished glass pipette, connected to an alternating electronic relay switch (Omron G2R-2-S) under the control of function generator (EZ digital) at 100-Hz rectangular wave function. The aCSF solution containing dissociated cells were collected and centrifuged at 1,000 rpm for 5 min. The collected cells were plated on 0.1 mg/mL PDL-coated cover glass, and placed in an incubator for about 2 h before use. The cell preparation including the time of stabilization was validated in previous studies (Lalo et al., 2011; Lalo et al., 2014; Lalo et al., 2006).

HEK293T cells, originated from Korean Cell Line Bank and mycoplasma free, expressing $GABA_CR$ and EGFP were added onto the cover glass with acutely dissociated cells. According to a previous report, astrocytes can be identified morphologically. To determine whether GFP-expressing HEK293T cells express $GABA_CR$, 100 μM GABA was bath-applied to induce $GABA_CR$-mediated full current. $GABA_CR$-mediated currents were recorded from HEK293T cells expressing $GABA_CR$ under voltage clamp (Vh = −70 mV) using Multiclamp 700B amplifier (Molecular Devices), acquired with pClamp 9.2. Recording pipettes were filled with (in mM): 140 CsCl, 0.5 $CaCl_2$, 10 HEPES, 4 Mg-ATP, 0.3 Na_3-GTP and 10 EGTA (pH adjusted to 7.3 with CsOH) and osmolality adjusted to 290–310 mOsm kg^{-1} with sucrose.

Flow Cytometry with acutely dissociated astrocytes

Flow cytometry was performed to confirm that acutely dissociated cells contain a significant portion of astrocytes, and the cell are live and functional. All flow cytometry experiments were performed on a BD LSRFortessa™ SORP with 5 lasers and 18 detectors (BD), controlled using FACSDiva™ software version 6, and was analyzed with using FlowJo V10 (BD). Debris and cell clumps were discriminated using forward scattering (FSC) and side scattering (SSC) gating.

Astrocyte phenotyping

The acutely dissociated cells were collected by and centrifuged at 1,000 rpm for 5 min. The cells were fixed in 4% PFA for 10 min at 4°C, then washed with stain buffer with BSA (554657, BD) for 2 times by repeating centrifugation at 2,500 rpm and re-suspension. Then, the fixed cells were incubated in the blocking buffer with 0.3% of Triton X-100 for 1 hour, and then labeled with a mixture of primary antibodies in a blocking solution at 4°C on a shaker overnight. The primary antibodies used for FACS analysis were chicken anti-GFAP (1:500; Millipore ab5541) and mouse anti-NeuN (1:1000; Millipore MAB377). After washing in stain buffer 3 times by repeating re-suspension and centrifugation at 3,000 rpm, the cells were incubated with corresponding fluorescent secondary antibodies for 1 h and then washed with blocking buffer 3 times. Finally one drop of 7-AAD (1581611, Bio-Rad) was added to the cell suspension and analyzed in order to discriminate dead cells. Flow cytometry analysis were preformed using of controls for determining appropriate gates, voltages and compensations required in flow cytometry.

Calcium flux measurement

To confirm that the acutely dissociated astrocytes are live and functional, Ca^{2+} flux analysis was performed using flow cytometry with Oregon Green 488 BAPTA-1 AM (O6807, Thermofisher Scientific). For Ca^{2+} flux analysis, the acutely dissociated cells were incubated with Oregon Green 5 μM solution in the external solution (150 NaCl, 10 HEPES, 3 KCl, 2 $CaCl_2$, 2 $MgCl_2$, 5.5 glucose, in mM, pH adjusted to pH 7.3.) for 30 min at 37°C. After incubation, cells were washed and then re-suspended in the external solution. The fluorescence in each sample was analyzed using 530/30 filter. Baseline calcium levels were recorded for 30 s on the cytometer. And the sample was removed and add TFLLR (50 μM) and immediately replaced for recording. After loading the compounds continued recording for 300 s. Ca^{2+} flux experiments were performed on live, non-fixed cells.

Whole-cell patch-clamp

Prior to recording, 300 μm-thick motor cortex-containing slices from freshly prepared brains were incubated at room temperature for at least 1 h in aCSF solution (in mM): 126 NaCl, 24 NaHCO3, 1 NaH2PO4, 0.5 ascorbic acid, 2.5 KCl, 2.5 CaCl2, 2 MgCl2, and 10 D-(+)-glucose, pH 7.4. For recording, slices were transferred to a recording chamber that was continuously perfused with aCSF solution (flow rate = 2 mL/min). The slice chamber was mounted on the stage of an upright Olympus microscope and visualized with a 60 × water immersion objective (NA = 0.90) with infrared differential interference contrast optics and a CCD camera and by using Imaging Workbench software (Indec BioSystems). Whole-cell recordings were performed from pyramidal neurons located in the layer 2/3 of motor cortex. The holding potential was −60 mV. Pipette resistance was typically 6–8 MΩ and the pipette was filled with an internal solution (in mM): 135 CsCl, 4 NaCl, 0.5 CaCl2, 10 HEPES, 5 EGTA, 2 Mg-ATP, 0.5 Na2-GTP, 10 QX-314, pH adjusted to 7.2 with CsOH (278–285 mOsmol). Before measuring tonic current, baseline current was stabilized with D-AP5 (50 μM) and CNQX (20 μM). Electrical signals were digitized and sampled at 50-ms intervals with Digidata 1440A and Multiclamp 700B amplifier (Molecular Devices) using pCLAMP 10.2 software. Data were filtered at 2 kHz. The amplitude of tonic GABA current was measured by the baseline shift after L655,708 (1 μM), NO-711 (10 μM), SNAP-5114 (40 μM), and/or bicuculline (50 μM) administration using the Clampfit program.

Frequency and amplitude of spontaneous inhibitory post-synaptic currents (sIPSCs) before bicuculline administration was detected and measured by Minianalysis (Synaptosoft). For the analysis of sIPSC frequency and amplitude, two cells from stroke+KDS group, whose Ra was over 40 MΩ, were excluded.

Electron microcopy and toluidine blue staining

Rat brains with diaschisis lesion in the microPET images were perfused with 1% paraformaldehyde/0.1% glutaraldehyde in cold phosphate buffer (PB) delivered by a perfusion pump (36 mL/min) for 5 min, followed by 2% paraformaldehyde/2% glutaraldehyde in cold PB at the same flow rate for 5 min. Brains were removed and coronally cut into 2-mm-thick slices. After the lesion was evaluated macroscopically in the brain slices, tissues were trimmed to approximately 2 × 2 × 1 mm, placed in 4% glutaraldehyde in PB for 24 h at 4°C, postfixed in 2% osmium tetroxide for 2 h at room temperature, rinsed in 0.1 mol/L cacodylate buffer, dehydrated in graded concentrations of ethanol followed by propylene oxide, incubated in a mixture of epon/propylene oxide (50/50, then 80/20 for 4 h), and embedded in epon at 60°C in an oven for 2 days. Semi-thin sections (1-μm-thick) were stained with 1% toluidine blue and screened by light microscopy to select thin section areas from multiple blocks at each lesion time-point for electron microscopy. Selected thin sections (800-A thick) were cut with a diamond knife on an ultramicrotome (LKB-Produkter, Bromma), mounted on copper grids, contrasted with uranyl acetate and lead citrate, and viewed on a JEOL 120S electron microscope.

For electron microcopy analysis, we used 2 sham animals and 4 stroke animals. For pathological examination and quantification of synapse numbers in the diaschisis, we only used tissues of motor cortex. Tissues of sensory cortex were excluded because optical fiber was introduced through sensory cortex. For quantification of synapse numbers, we used 24 and 29 motor cortex sections from 2 sham and 4 stroke animals, respectively. The analyses were performed in a blinded manner by two independent neuropathologists.

Drug administration

KDS2010, a MAO-B inhibitor, was synthesized as previously descried (Park et al., 2019). Rats were habituated with 0.9% saline for 2 weeks prior to surgery. The compound was dissolved in distilled water and administered through oral route (10 mg/kg daily) for 3 weeks from 3 days following stroke operation in Stroke+KDS2010 and Stroke+rehab+KDS2010 group. To test the effect of KDS2010 in Adeno-GFAP-GFP-injected rats, we administered KDS2010 from 3 days prior to virus injection to 1 week following virus injection through dissolving the compound in drinking water. The amount of KDS2010 was calculated as 10 mg/kg daily. To test the effect of L655,708 in stroke rats and Adeno-GFAP-GFP-injected rats, we intraperitoneally administered L655,708 (5 mg/kg) for once 30 minutes prior to FDG administration on the day of PET imaging.

Measurements of MAO-B enzyme activity

The enzymatic activity of MAO-B was measured as previously described (Jo et al., 2014). Rats were anesthetized and then the brain was quickly excised from the skull and submerged in ice-cold cutting solution, which is the same as the cutting solution for tonic GABA recordings. After cooling, cortical regions including somatosensory and motor cortex were isolated. The fresh tissues from each rat were homogenized, and large debris was removed by weak centrifugation. Next, the supernatant was collected and centrifuged at 13,000 rpm for 20 min to obtain a mitochondria-rich fraction. The pellet was re-suspended in phosphate buffer, and 20 mg were used in each well to determine the activity of the Mao. Enzymatic activity of MAO-B was measured using an Amplex Red Monoamine oxidase Assay Kit (Molecular Probes) according to the manufacturer's instructions. After 30 min of enzyme reaction at 37°C, hydrogen peroxide, which is produced by MAO activity, is measured by a color change of Amplex red reagent. The color change was quantified by measuring absorbance at 570 nm with Infinite M200 PRO microplate reader (TECAN).

Behavioral testing

Two types of behavioral tests were used in this study: the forelimb-use asymmetry test (cylinder test) was used to assess unskilled motor behavior and the single-pellet reaching task (SPRT) was used to assess skilled motor behavior. To perform the cylinder test (Hsu and Jones, 2005; Hua et al., 2002), animals were placed in a transparent Plexiglas cylinder (20 cm in diameter and 30 cm in height) for two minutes to assess the frequency of usage of ipsilesional and contralesional forelimb to support an upright body posture against the wall of the cylinder. We counted the number of ipsilateral and contralateral forepaw usages for each session. The test score was calculated as the percentage of the number of ipsilateral usage to the total number of ipsilateral and contralateral usages. For SPRT evaluation (Gharbawie et al., 2005), we used a clear Plexiglas (45 cm × 13 cm × 40 cm) box with a 1 cm wide vertical slit and food shelf in the midline of the frontal wall. During the entire experimental period, animals were food-restricted to 90% of their body weight for motivating food retrieval. The preferred handedness of each rat was determined during the pre-training by evaluating how successful the preferred paw was in retrieving sucrose pellets (Bio-Serve) that had been placed obliquely on the shelf. A successful reach was considered if the rat extended a forelimb to grasp the pellet, and brought it into the mouth without dropping it. The animals were administered 20 pellets per session for evaluation of motor performance. The reaching performance was calculated as follows:

$$\frac{\textit{Number of successful reaches} \times 100}{20}$$

Animals were trained daily for two weeks before photothrombotic stroke lesioning. Animals in the rehabilitation group (Stroke+rehab, Stroke+rehab+KDS2010) and the sham group underwent daily postoperative training for 20 min for three weeks. Animals in the non-rehabilitation groups (Stroke and Stroke+KDS2010) performed the reaching task twice per week for three weeks postoperatively and on the day of sacrifice (i.e, a total of 6 post-operative training sessions). The analyses were performed by a blinded researcher.

Preparation and injection of putrescine and viruses

The MAO-B shRNA sequence (antisense) is AATCGTAAGATACGATTCTGG. For lentivirus-based shRNA expression, a lentiviral vector containing the MAOB-shRNA gene was constructed into the HpaI–XhoI restriction enzyme sites of the pSicoR lentiviral vector, as previously described (Yoon et al., 2014). To selectively knockdown astrocytic MAO-B, we injected AAV-GFAP-Cre-mCherry and lentivirus containing pSico-MAOB-shRNA-GFP (or pSico-scrambled-shRNA-GFP for control) into the forelimb area of the motor cortex (AP = −2.0 mm, ML = +/− 2.5 mm, DV = −1.5 mm from bregma), using techniques as previously described (Song et al., 2017). A mixture of 1 μL of AAV and 1 μL of lentivirus virus was slowly injected at the target site (layer 5 of forelimb area) with a rate of 0.1 ml/min using 30G Hamilton syringe connected to an UltraMicroPump (WPI). After injection, the needle was left in place for an additional 10 min before being slowly retracted. Postoperative pain was controlled with ketoprofen (2 mg/kg, i.m.).

To induce neuroinflammation including reactive astrocytosis with aberrant astrocytic GABA production, we developed Adeno-GFAP-GFP plasmid. As a GFAP promoter, we used gfaABC1D promoter which is reported to be highly specific to astrocytes (Lee et al., 2008). We prepared pAd-GFAP-GFP using Gateway® gene cloning strategy. In detail, we first excised gfaABC1D-EGFP from pTYF-1xGfaABC1D-EGFP (Addgene, #19974). Next, for constructing a packaging backbone plasmid containing attB recombination sites for the shuttle vector plasmid to be recombined into, we obtained attB1-GFAP-GFP-attB2 sequence through PCR with primer containing attB1 and attB2. Then, Gateway® BP reaction was performed using this attB1-GFAP-GFP-attB2 sequence and pDonor vector (Invitrogen, 12536017) to obtain pDonor-GFAP-GFP plasmid. Finally, Gateway® LR reaction was performed using this plasmid with pAd/PL-DEST vector (Invitrogen, V49420) to obtain pAd-GFAP-GFP plasmid.

To confirm whether astrocytic GABA induces cortical diaschisis, we injected 2 μL of Adeno-GFAP-GFP (N = 8) or 2 mM putrescine (N = 8) into the forelimb area of the motor cortex (AP = −2.0 mm, ML = +/− 2.5 mm, DV = −1.5 mm from bregma) using techniques in a same way. Animals in the control group (N = 8) underwent the same procedure except that they received an injection of 0.9% saline (2 μL) instead of Adenovirus and putrescine. To investigate whether KDS2010 and L655,708 reverses Adeno-GFAP-GFP-induced decrease in FDG uptake, we injected 1.5 uL of Adeno-GFAP-GFP into M1 motor cortex (AP = −0.2 mm, ML = +/− 2.0 mm, DV = −1.5 mm from bregma) and S1 somatosensory cortex (AP = −0.2 mm, ML = +/− 4.0 mm, DV = −2.5 mm from bregma).

To induce a severe lesion in the cortex, we injected 2 uL of 100 mM putrescine into five consecutive points into the motor cortex (1: AP = −0.5 mm, ML = +1.5 mm from bregma, DV = −1.3 mm from dura; 2: AP = +1.0 mm, ML = +3.0 mm from bregma, DV = −1.3 mm from dura; 3: AP = +2.0 mm, ML = +2.5 mm from bregma, DV = −1.3 mm from dura; 4: AP = +3.0 mm, ML = +1.5 mm from bregma, DV = −1.3 mm from dura; 5: AP = +3.0 mm, ML = +4.0 mm from bregma, DV = −1.3 mm from dura). Animals in the control group (N = 8) underwent the same procedure except that they received an injection of 0.9% saline (2 μL) instead of putrescine.

Quantitative real-time RT-PCR

Quantitative real-time RT-PCR was carried out using SYBR Green PCR Master Mix. In brief, reactions were performed in triplicates in a total volume of 10 mL containing 10 pM primer, 4 mL cDNA, and 5 mL power SYBR Green PCR Master Mix (Applied Biosystems). The mRNA level of each gene was normalized to that of *Gapdh* mRNA and fold-induction was calculated using the 2–DDCT method. The following sequences of primers were used. *Gfap* forward: 5′-GAA GAA AAC CGC ATC ACC AT-3′; *Gfap* reverse: 5′-*TCC TTA ATG ACC TCG CCA TC*-3′; *Maob* forward: 5′-CGA GAC AGC TTC ACA TTG GA-3′; *Maob* reverse: 5′-GCC AAA TTT CAT CCT CTG GA-3′; *Inos* forward: 5′-CCT GTG TTC CAC CAG GAG AT-3′; *Inos* reverse: 5′-CGC TTT CAC CAA GAC TGT GA-3′; *Lcn2* forward: 5′-TCA CCC TGT ACG GAA GAA CC-3′; *Lcn2* reverse: 5′-TCG GTG GGA ACA GAG AAA AC-3′; *Vimentin* forward: 5′-AGA TCG ATG TGG ACG TTT CC-3′; *Vimentin* reverse: 5′-TCC GGT ATT CGT TTG ACT CC-3′; *C3* forward: 5′-GAA GCC CTA GTG GGG AAG TC-3′; *C3* reverse: 5′-AAC ACC ATG AGG TCG AAA GG-3′; *Gapdh* forward: 5′-ACC CAG AAG ACT GTG GAT GG-3′; *Gapdh* reverse: 5′-CAC ATT GGG GGT AGG AAC AC-3′.

QUANTIFICATION AND STATISTICAL ANALYSIS

Image quantification

Confocal microscopic images were analyzed using the ImageJ program (NIH).. For analyzing GABA intensity in $GFAP^+$ astrocytes or PV^+ interneurons, every image was first converted to 16-bit image, then converted into binary. Every $GFAP^+$ astrocyte or PV^+ interneuron was picked as a region of interest (ROI). And the binary $GFAP^+$ image and $GABA^+$ image were multiplied to remaining $GABA^+$ signal only in the $GFAP^+$ pixels. In this multiplied image, the mean intensity value of GABA in every ROI was measured. Quantification of LCN2 intensity in $GFAP^+$ astrocytes was performed in the same way as quantification of GABA intensity. For quantifying $GFAP^+$ area of a $GFAP^+$ astrocyte, we measured mean intensity from 16-bit binary $GFAP^+$ image. To quantify the reactivity of astrocytes, we performed Sholl analysis with a plugin provided by ImageJ program. To perform Sholl analysis, we used the ROIs described above from 16-bit binary $GFAP^+$ images. Radius step size was 10 μm and the number of primary branches were automatically inferred from starting radius.

Statistical analyses

Data were analyzed with Prism 7 (GraphPad). Time-dependent changes in cortical diaschisis volume, NMA, and behaviors were analyzed using two-way ANOVA ($p < 0.05$, Bonferroni correction for multiple comparisons). Differences between two different groups were analyzed with the two-tailed Student's unpaired t test. For assessment of change of a group by a certain intervention, the significance of data was assessed by the two-tailed Student's paired t test. For comparison of multiple groups, one-way analysis of variance (ANOVA) with Tukey's or Dunnett's multiple comparison test was assessed. All data are represented as mean ± standard error of the mean (SEM). The significance level is represented as asterisks (*$p < 0.05$, **$p < 0.01$, ***$p < 0.001$; ns, not significant).

For the longitudinal PET study, a group-level linear mixed-effect model was performed with the 3dLME program of AFNI to assess differences between baseline (PL −1) and PL 7, 14, and 21 images for each group of animals. Statistical maps were corrected and thresholded at the significance level ($p < 0.001$, false discovery rate $q < 0.05$). In addition, we conducted a voxel-wise paired t test with 3dttest in AFNI to compare pre-injection versus post-injection scan (AAV, putrescine, and saline injection groups). Monte Carlo simulation was used with 3dClustSim program in AFNI, and statistical maps were thresholded at $p < 0.01$ and the minimum cluster size of 39 voxels with $p < 0.05$. The resulting statistical maps overlaid on the template to show areas of significant brain activity changes. An ROI was manually defined in ipsilesional motor cortex to identify the longitudinal changes of NMA. In addition, using Pearson's correlation ($p < 0.05$), we examined correlations between NMA changes in ROI and intensity of astrocytic GABA, and correlations between NMA changes or volume of cortical diaschisis and SPRT scores.